BACHELOR THESIS

EXPERIMENTAL EVALUATION OF MAGNETIC ACTUATION OF A 3D SHAPE MEMORY ORIGAMI STRUCTURE

WOUTER KOETSIER

FACULTY OF ENGINEERING TECHNOLOGY
DEPARTMENT OF BIOMECHANICAL ENGINEERING

EXAMINATION COMMITTEE
PROF. DR. S. MISRA
DR. V. KALPATHY VENKITESWARAN
DR. H.K. HEMMES

DOCUMENT NUMBER
BE-974

JANUARY 18, 2024

UNIVERSITY OF TWENTE.

Thesis submitted by
Wouter Koetsier
under the supervision of
Prof. dr. S. Misra,
dr. V. Kalpathy Venkiteswaran, and
dr. H.K. Hemmes
in order to fulfil the necessary requirements to obtain a Bachelor's degree in
Advanced Technology at the University of Twente
and defended on
Thursday, January 18, 2024

SURGICAL ROBOTICS
LABORATORY

WWW.SURGICALROBOTICSLAB.NL

Abstract

Minimal Invasive Surgery (MIS) is a field of study that aims to improve patients' safety and reduce post-operative complications. One promising approach to designing new tools and devices for MIS is using Shape Memory Polymer (SMP) origami structures. Using magnetic actuation, the shape memory origami can be controlled and manipulated. However, before this can be achieved, the behaviour of the SMP origami structures needs to be studied. In this research, the focus is on an L-shaped origami structure and its three-dimensional movements. This research aims to predict the response of the L-shape structure when magnets are attached and placed in a magnetic field. The studied L-shape structure has three square panels separated by engraved hinges. One panel is fixed to the outside world, while the other two panels can bend around the hinges. This study has involved modelling and producing the structure to experiment with and hypothesise the results. Initially, the assumption was made that the structure would only bend at the hinges in one direction. However, experiments have shown that the SMP origami structure also twists around the hinges. This means that more research needs to be done to improve the understanding of SMP origami structures.

Table of Contents

List of Figures

List of Tables

1 Introduction

Present-day, about 310 million major surgeries a year are being performed worldwide [3]. Formerly, most surgeries were exposed operations with extensive incisions. Larger incisions and more blood loss can cause postoperative complications [4]. To reduce these incisions and the risk of complications, the focus of research has been on Minimally Invasive Surgery(MIS) in the past decades [5]. For example, laparoscopy was performed for the first time a little more than a century ago [6]. More research is being done on improving MIS and developing new methods and tools.

For MIS, it is essential to keep the size of the surgical tools to a minimum. However, while minimizing the size, the functionality of a tool should not be limited as these tools are designed to perform a specific task with it. A promising material for these tools is Shape Memory Polymer (SMP) [7].

A significant advantage of SMP is its shape memory characteristic. The material can be deformed plastically by applying an external force. After deformation, its original shape can be recovered by applying a stimulus on the material. The recovery stimulus can differ per SMP type. Examples of stimuli are recovery by using heat, electric-induced recovery, and light-induced recovery. This effect is known as the Shape Memory Effect [8]. This effect could be beneficial for targeted drug delivery systems by using this recovery effect to release the medicine at the medicine's targeted location.

Other advantages of SMP are its wide range of transition temperatures, low cost, biodegradability, and high elastic deformation [7]. These advantages make this material very suitable for developing new surgical devices.

When designing these tools with SMP, origami, the art of folding, could be an excellent inspiration. Origami is already being used for different biomedical applications. For example, origami-inspired drug delivery systems or origami-inspired stents and catheters [9], [10]. The biggest challenge for designing devices in such a manner is manipulating and transporting origami shapes inside the human body because applying an external stimulus to the material is hard while operating.

Magnetic actuation could be a solution to the manipulation and transportation challenges [11]. A magnetic field can be generated from outside of the human body without causing any trauma to the body. For example, Magnetic Resonance Imaging scans, which are widely used in the medical field [12]. This makes it possible to use magnetic fields to control small medical robots or devices.

To control a Shape Memory Origami using magnetic actuation, it is necessary to have a better understanding of these effects and predict its behaviour. This study will focus on these effects. In previous studies [13], [14], the behaviour of magnetic activation of 2-dimensional shape memory origami structures has been evaluated. Evaluation has been done using both simulations and experiments. In both simulations and experiments, they were able to create a V shape from two panels. However, in practice, it was harder to realize more complex structures, like a zigzag structure with more than two panels. This is expected to be because of internal interactions between multiple magnets [14]. However, this study will step away from the zigzag structure and instead focus on Shapes in 3 dimensions.

At the beginning of this research, some analysis has to be performed on magnetically actuating a 3d shape memory origami structure. This is done to predict how the structure will behave. In this thesis, the focus is put on an L-shape made out of 3 square panels divided by two folding lines. The SMP L-shape origami must be designed and produced to test this analysis. To test the samples, the origami structures will be fixed on one side and have magnets attached to each bendable panel. The samples will be placed in a magnetic field generator, and changing the current through the Helmholtz coils of the magnetic field generator will vary the strength and direction of the magnetic field applied to the sample. The final goal of this research is to predict the behaviour of a 3d L-shape memory origami structure. This understanding could predict the behaviour of more complex 3d shapes.

2 Theoretical Background

This section provides background theory to understand the magnetic actuation of 3D-shaped memory origami structures. Furthermore, it includes an analysis of an L-shape origami structure and explanations of a model of this shape.

2.1 Shape Memory Polymers

Shape Memory Polymers (SMPs) are elastic polymer networks. These polymer networks have a permanent state that, after plastic deformation, can be recovered by an external stimulus. This recovery effect is called the shape memory effect, and it is caused by molecular structure switches, which are activated by external stimuli like electricity or heat [1].

The permanent state is determined by network points in the polymer network. These points are formed during the manufacturing of the material [1]. This means that the state in which the material is produced is its permanent state, meaning that the permanent state of the SMP can be chosen by making the material in the desired permanent shape.

SMP can be plastically deformed, going from its permanent state to a temporary state using mechanical force. This is called programming, and by using a stimulus, it can return to its permanent state; this is called recovery. These two steps together form a cycle.

An example of such a cycle for a SMP is given below in Fig. 1. The material starts above its transition temperature, activating it to stay in its permanent state B. By applying a force to the material and cooling the SMP, the material is elongated to state A and kept. The material can be kept in this state by keeping it under its transition temperature. Then, by heating the SMP to above its transition temperature, it recovers to shape B.

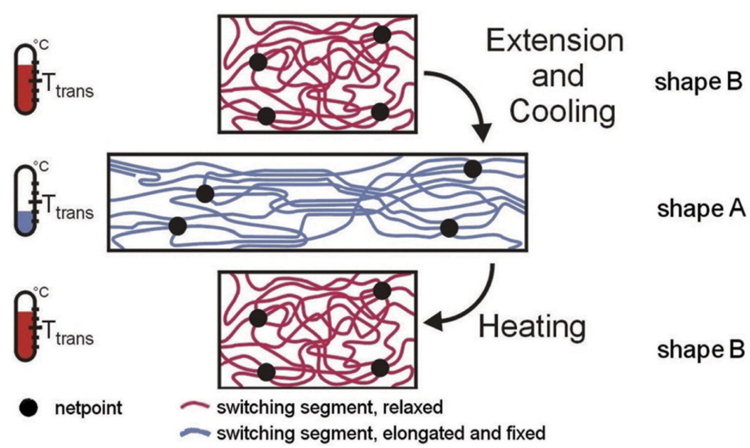

Figure 1: A shape memory effect cycle [1] going from state B to state A by mechanical force and back to state B by heating.

For this research, the SMP DiAPLEX is used. DiAPLEX is a commonly used SMP [15]. DiAPLEX is a highly elastic SMP with a thermal recovery activation. With a glass transition temperature ranging from 25°C to 90°C., DiAPLEX comes in three different types: a pellet type, MM, a solution type, MS, and a resin and hardener type, MP.

For this research, the MP type has been used. DiAPLEX MP type is produced in 4 different types, MP2510, MP3510, MP4510, and MP5510, each having other material properties. MP3510 has been selected because it has a glass transition temperature of 35°C [15]. This temperature is slightly below the human body temperature, and it is pretty easy to heat the sample to above it.

2.2 Magnetic Actuation

Magnetic actuation is a technology that uses magnetic fields to control the movement of magnetic objects using electromagnets or permanent magnets. It offers precise and non-contact actuation [11]. Making it very suitable for steering and bending SMP materials within the human body [4].

When a magnetic field is applied to a magnetic object, it generates both a force and a torque. The magnetic force can be quantified by integrating the dot product of the magnetic density per unit volume and the curl of the magnetic field across the magnet's volume, Eqn. (1). The magnetic torque is ascertained by integrating the cross-product of the magnetic density per unit volume and the magnetic field over the volume of the magnet, Eqn. (2).

$$\vec{F_m} = \int_V (\vec{M} \cdot \nabla \vec{B}) dV. \tag{1}$$

$$\vec{\tau_m} = \int_V (\vec{M} \times \vec{B}) dV. \tag{2}$$

In Eqns. (1)-(2) $\vec{M}$ represents the internal magnetization per unit volume of a permanent magnet, while $\vec{B}$ denotes the external magnetic flux field applied to actuate the magnet. Given the magnet's relatively small size, both ∇B and B will be assumed constant during the integration across the magnet's volume. This simplifies the Eqns. (1)-(2) into Eqns. (3)-(4).

$$\vec{F_m} = \vec{m} \cdot \nabla \vec{B}. \tag{3}$$

$$\vec{\tau_m} = \vec{m} \times \vec{B}. \tag{4}$$

Two options exist for generating an external magnetic field for magnetic actuation: permanent magnets or electromagnetic coils. In this research, electromagnetic coils are chosen due to their ease of control over the strength and orientation of the applied magnetic field. This is essential for achieving precise control of the SMP.

In this research, a homogeneous magnetic field will be applied to the magnets. This means that everywhere in the magnets' operating space, the external magnetic field lines will be parallel and of equal strength for each moment in time. In regions where the magnetic field is homogeneous, the curl of the field is zero, indicating the absence of magnetic forces acting upon the magnets. This means that only a torque will be generated.

2.3 Analysis L-shape Structure

In previous research, 2D origami shapes have been analysed [13], [14]. From a single panel to a more complex zigzag structure. This study focuses on a 3D shape, an L-shape consisting of three panels and two hinges, as shown in Fig. 2. One of the three panels of the L-shape will be fixed to a frame, and the other two panels will be free to rotate around the hinges. This gives the shape 2 degrees of freedom.

A magnet will be placed in the middle of each panel with a dipole moment $\vec{m}$. This moment can be determined by Eqn. (5). With V being the volume of the magnet $\vec{B_r}$ the residual flux density and μ_0 the permeability of vacuum, being $4\pi \cdot 10^{-7}$ N/A^2.

$$\vec{m} = \frac{V \cdot \vec{B_r}}{\mu_0}. \tag{5}$$

To create hinges, the material will be engraved with a laser cutter, creating notches in the material at locations indicated in Fig. 2. These notches cause the material to be more flexible at the hinges than the other parts, causing it to bend only at the desired locations.

These hinges are expected to behave like a rotation spring with a spring constant. This constant can be calculated with Eqn. (6). With E being Young's modulus of the material, I the moment of inertia of the hinge, and L the length of the hinge.

$$K = \frac{EI}{L}. \tag{6}$$

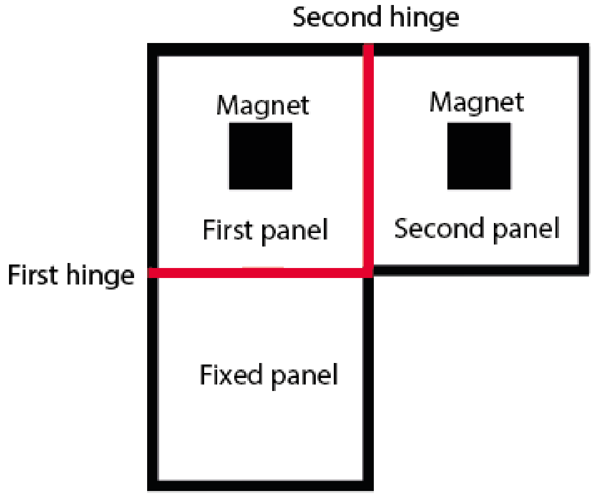

Figure 2: An L-shaped origami structure with two hinges and magnets placed on the two bending panels.

The moment of inertia of the hinge can be determined with Eqn. (7). b is the width of the hinge, and h is the height of the hinge. Fig. 3 shows a single hinge's width, height, and length.

$$I = \frac{bh^3}{12}. \tag{7}$$

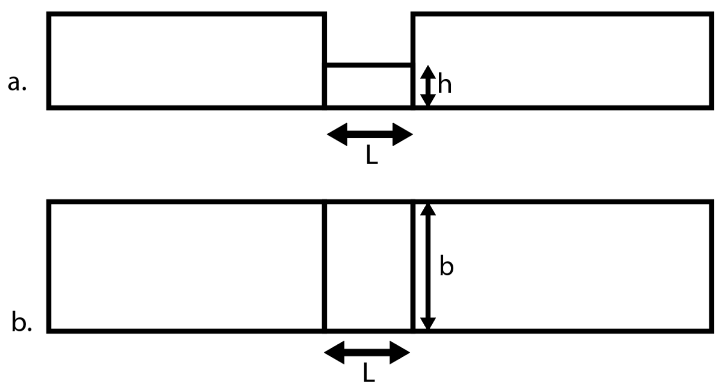

Figure 3: a. Shows a side view of a single hinge, b. Shows a top view of a single hinge.

When applying a magnetic field on the L-shape of Fig. 2, torques are applied to each magnet. These torques will force the structure to bend around its hinges. These bendings introduce a reaction force of the hinges wanting to move back to their permanent state because of the memory effect of the SMP.

Eqn. (4) can be used to determine the torques acting on the magnets. However, the orientations of the magnets change as the panels start to bend because they are fixed to the panels. For this reason, reference frames are introduced, as shown in Fig. 4. S_0 is the reference frame fixed to the outside world and the clamped panel. S_1 is fixed to the first bending panel, and S_2 is fixed to the second bending panel. Both hinges have an angle expressed in α_1 as shown in Fig. 4b, and α_2 as shown in Fig. 4c.

The dipole moment of magnet 1, $\vec{m}_1$, can be easily expressed in the reference frame fixed to the first panel, S_1. In the same way, the dipole moment $\vec{m}_2$ can be easily expressed in reference frame S_2. However, to determine the torques acting on these magnets, the dipole moments must be expressed in the outside-world reference frame, S_0. This has been done by the use of rotation matrices.

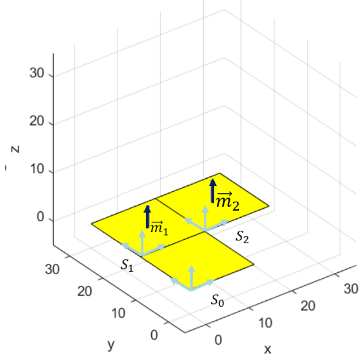

(a) The L-shape with reference frames without any bending.

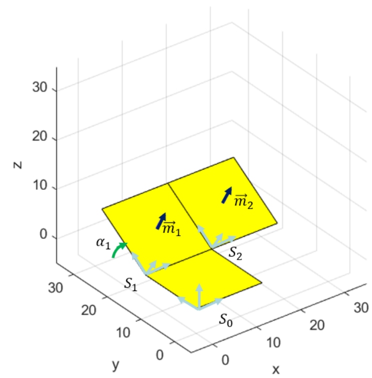

(b) The L-shape with reference frames bending around the first hinge with angle α_1.

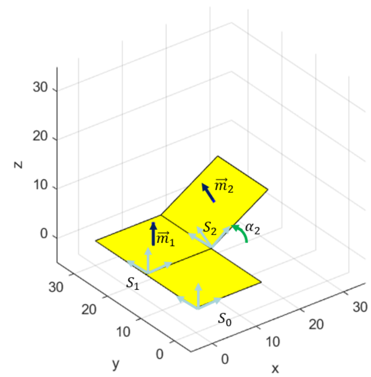

(c) The L-shape with reference frames bending around the first hinge with angle α_2.

Figure 4: An L-shaped structure with reference frames with different bendings.

Rotation matrices are tools used to transform points or vectors from one reference frame to another. In a three-dimensional space, there are three standard rotations. A rotation around the x-axis with angle θ, Eqn. (8), a rotation around the y-axis with angle θ, Eqn. (9), and a rotation around the z-axis with angle θ, Eqn. (10).

$$R_x(\theta) = \begin{bmatrix} 1 & 0 & 0 \\ 0 & \cos(\theta) & -\sin(\theta) \\ 0 & \sin(\theta) & \cos(\theta) \end{bmatrix}. \tag{8}$$

$$R_y(\theta) = \begin{bmatrix} \cos(\theta) & 0 & \sin(\theta) \\ 0 & 1 & 0 \\ -\sin(\theta) & 0 & \cos(\theta) \end{bmatrix}. \tag{9}$$

$$R_z(\theta) = \begin{bmatrix} \cos(\theta) & -\sin(\theta) & 0 \\ \sin(\theta) & \cos(\theta) & 0 \\ 0 & 0 & 1 \end{bmatrix}. \tag{10}$$

The L-shape Structure has a rotation around the first hinge parallel to the x-axis. The rotation is measured clockwise and expressed as α_1 as depicted in Fig. 4b. The rotation matrix will be from frame S_1 to frame S_0, and the positive rotating direction is counter-clockwise. From this, rotation matrix R_1 can be formed, Eqn. (11).

The rotation around the second hinge is parallel to the y-axis. So, the rotation matrix for this hinge will be similar to Eqn. (9). The angle α_2 is the difference between the first and second penal, as shown in Fig. 4c.

This angle is measured in the positive rotating direction, counter-clockwise. The second rotation matrix will be from S_2 to S_1, meaning the rotating angle is $-\alpha_2$. This gives the second rotation matrix Eqn. (12)

$$R_1(\alpha_1) = \begin{bmatrix} 1 & 0 & 0 \\ 0 & \cos(\alpha_1) & -\sin(\alpha_1) \\ 0 & \sin(\alpha_1) & \cos(\alpha_1) \end{bmatrix}. \tag{11}$$

$$R_2(\alpha_2) = \begin{bmatrix} \cos(\alpha_2) & 0 & -\sin(\alpha_2) \\ 0 & 1 & 0 \\ \sin(\alpha_2) & 0 & \cos(\alpha_2) \end{bmatrix}. \tag{12}$$

Using these matrices, the orientation of the magnets can be determined in the outside world frame S_0, as shown in Eqns. (13)-(14)

$$\vec{m_1^0} = R_1(\alpha_1) \cdot \vec{m_1^1}. \tag{13}$$

$$\vec{m_2^0} = R_1(\alpha_1) R_2(\alpha_2) \cdot \vec{m_2^2}. \tag{14}$$

The hinges of the origami shape will be modelled as rotational springs with a spring constant K for rotations around the hinge. It is assumed that bending occurs only at the hinges and in one direction per hinge, α_1 and α_2. With this assumption, the two hinges can be modelled like Eqns. (15)-(16).

$$\tau_{k1} = -K\alpha_1. \tag{15}$$

$$\tau_{k2} = -K\alpha_2. \tag{16}$$

A force equilibrium can be described using the torques, the rotation matrices, and the magnetic actuation. Since the sample is fixed on one side, it will not translate but only rotate. For this reason, the sample will be modelled using two torque summations and no force summations, one summation around the first hinge and one around the second hinge.

When a magnetic field is applied, the x components of the torques on both magnets, $(\vec{\tau}_{m1})_x$ and $(\vec{\tau}_{m2})_x$, force the sample to bend around the first hinge creating a reaction force from the hinge τ_{k1}. Eqn. (17) shows the torque summation around the first hinge with α_1 as the positive rotating direction. For the second panel, the torque working on the second magnet has a component parallel to the hinge, causing it to bend. To find the component parallel to the hinge. The torque must be translated back to the reference frame of panel 1 S_1, using the transpose of rotation matrix $R_1(\alpha_1)$. This is because the hinge is attached to the first panel. Eqn. (18) shows the torque summation at the second hinge with α_2 as the positive rotating direction.

$$\sum \tau_{hinge1} = (\vec{\tau}_{m1})_x + (\vec{\tau}_{m2})_x - \tau_{k1}. \tag{17}$$

$$\sum \tau_{hinge2} = \left(R_1^T(\alpha_1) \cdot \vec{\tau}_{m2}\right)_y - \tau_{k2}. \tag{18}$$

For this research, interests lie only in the final states of the sample. Therefore Eqns. (17)-(18) are equal to 0. By combining in Eqns. (13)-(14) with Eqn. (4) and filling these equations together with Eqns. (15)-(16) into Eqns. (17)-(18). The equilibrium equations become Eqns. (19)-(20).

$$\left(R_1(\alpha_1)\vec{m_1^1} \times \vec{B^0}\right)_x + \left(R_1(\alpha_1)R_2(\alpha_2)\vec{m_2^2} \times \vec{B^0}\right)_x = K\alpha_1. \tag{19}$$

$$\left(R_1^T(\alpha_1)\left(R_1(\alpha_1)R_2(\alpha_2)\vec{m_2^2} \times \vec{B^0}\right)\right)_y = K\alpha_2. \tag{20}$$

2.4 Model

The Equilibria Eqns. (19)-(20) can be used to predict the behaviour of the sample when the orientation of the magnets is selected, and a specific magnetic field is applied. These equations are rather complex as they contain multiple matrix and vector multiplication. Matlab is a powerful tool for solving these equations because it has equation solver tools and can easily do matrix and vector multiplications. Therefore, a model has been built in Matlab.

In Fig. 4, a few bendings are shown. These bendings have been predicted with the Matlab model. In Fig. 4a, no magnetic field is applied; in Fig. 4b, a magnetic field is applied in the negative Y direction, and in Fig. 4c, a field is applied in the negative X direction. Fig. 5 shows the model with a double bending, one on each hinge. In this figure, a magnetic field is applied in the minus X and minus Y direction, having vector $(-1, -1, 0)$ with a strength B.

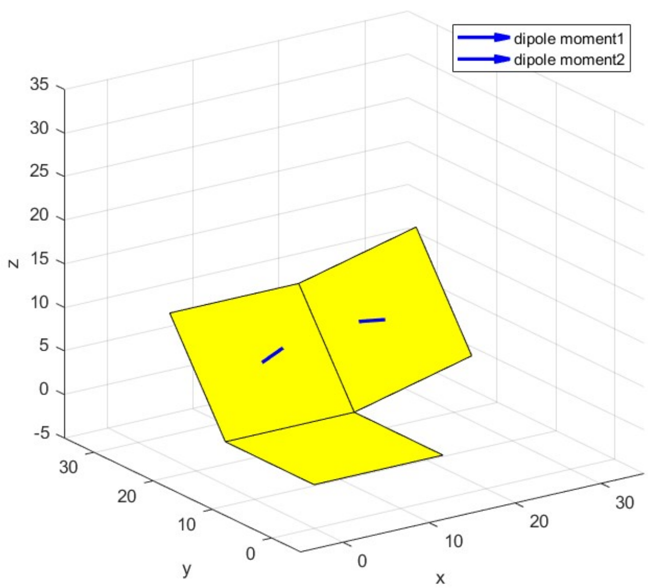

Figure 5: L-shape with a magnetic field applied in the (-1,-1,0) direction.

The model has been used to predict the behaviour of the sample when applying the magnetic field in a specific direction and changing the strength of the magnetic field. Fig. 6 shows the expectation of bending when using a magnetic field with the direction vector $(-1, -1, 0)$.

The curve has an S-shape. This could be explained by the fact that the torque applied to the magnets tries to align the magnetic dipole moments with the lines of the magnetic field. As a result, the panels bend the angle between the magnetic dipole moment and the magnetic field becomes smaller. As a consequence, the torque applied on the magnet increases with smaller steps because the torque is a cross-product of the two vectors, $\vec{m}$ and $\vec{B}$.

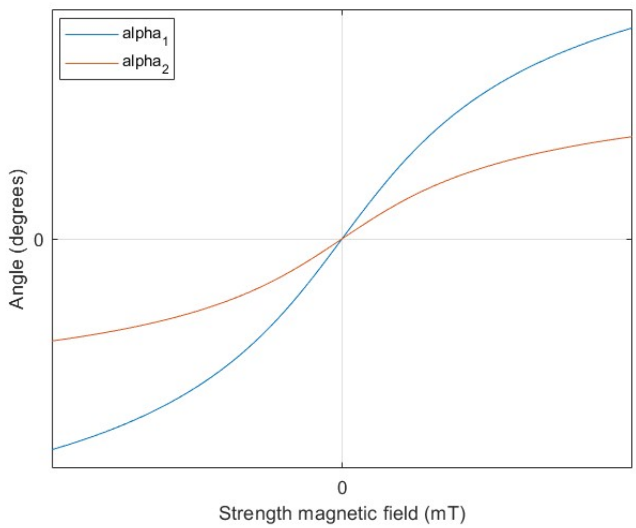

Figure 6: Expectation bending curve of the L-shape when applying a magnetic field in the -(-1,-1,0) direction.

3 Methods

This section explains the methods used to test the theories, describes the production methods used to create the L-shaped sample, and methods used to test the predictions of the theory of section 2.

3.1 Materials and Fabrications

This study used SMP DiAPLEX because it has a low glass transition temperature and is very flexible. However, while producing samples of this material, some problems arose. For this reason, another material has been chosen to make the sample and experiment with. Production methods used for the SMP DiAPLEX and issues that arose are described in the appendix A.1.

The material Norland Optical Adhesive 63 (NOA63) [16] has been used in the following experiments. This material is made for optical adhesive purposes but also has thermal shape memory properties. It has been decided to make the L-shape samples out of this material because it is very straightforward to make clean samples out of NOA63. However, this material is more brittle than DiAPLEX, making it less flexible and tearing faster, which is undesirable when used to design medical tools. However, since it will behave similarly to DiAPLEX, it can be used to understand the origami L-shape.

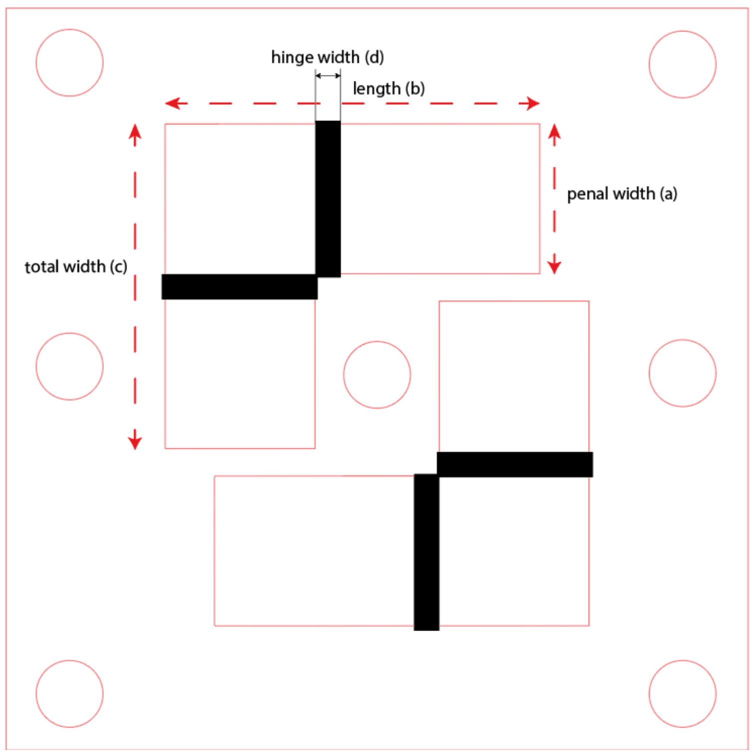

Figure 7: A the mold used to make L-shaped SMP samples. The red lines indicate the cutting lines, and the black lines indicate the engraving lines for the hinges. The dashed lines are used to indicate the dimensions.

The following steps have been used to make the samples with NOA63. First, a mold was made out of 2 mm thick plexiglass, as shown in Fig. 7. Dimensions of the mold and sample are shown in Table 1. Next, the mold was put together and filled with liquid NOA63. To curate the sample, it was placed under UV light. It was put in a laboratory oven for 30 minutes with the nail UV light to curate at 40°C. This temperature was chosen because the temperature at which the sample was curated is close to the activation temperature of the memory effect of the SMP sample.

Once the sample has been curated, it is engraved with a laser cutter to create hinges. Table 2 shows the settings used to engrave the hinges. It has been done in multiple cycles with low power and high speed

Table 1: Sample dimension as defined in Fig. 7.

Dimension	Value (mm)
Sample thickness	2
Panel width(a)	9
Length (b)	22
Total width (c)	20
Hinge width (d)	2
Hinge depth	1

to create cleaner engravings. Engraving with fewer cycles but higher power and lower speed creates less accurate engravings, and it tends to melt the material, which might influence its properties.

Table 2: Settings used for engraving the hinges in the sample.

Cycles	Velocity (m/s)	Power (%)
4	10	20
3	10	30

Once the hinges have been engraved, the magnets are attached to the middle of each panel. This has been done using super glue. For this thesis, N48 neodymium block magnets have been used. These magnets have a residual flux density of $\vec{B_r} = (14{,}0 \pm 0.2)$ KGs, and the magnets used have the dimensions of 5 mm by 5 mm by 1 mm. Using Eqn. (5), the magnitude of the dipole moment is $m \approx 2.7$ mT and has a direction normal to its 5 mm by 5 mm side.

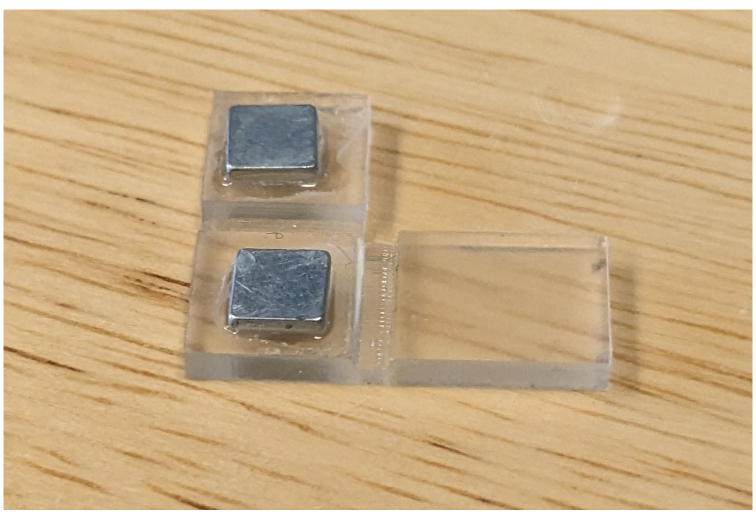

Figure 8: An L-shape NOA63 sample with engraved hinges and N48 neodymium block magnets.

Fig. 8 shows an example of a finished L-shape sample. Here, the magnetic dipole moments are both pointed upwards normal to the panel's plane.

3.2 Setup

A setup must be designed to test the L-shape sample and measure the results. This setup requires the possibility of generating a homogeneous magnetic field over the whole operating space of the sample. Next, the sample needs to be kept at a temperature above the glass transition temperature. The final requirement of the setup is the possibility to measure both bending angles of the L-shape.

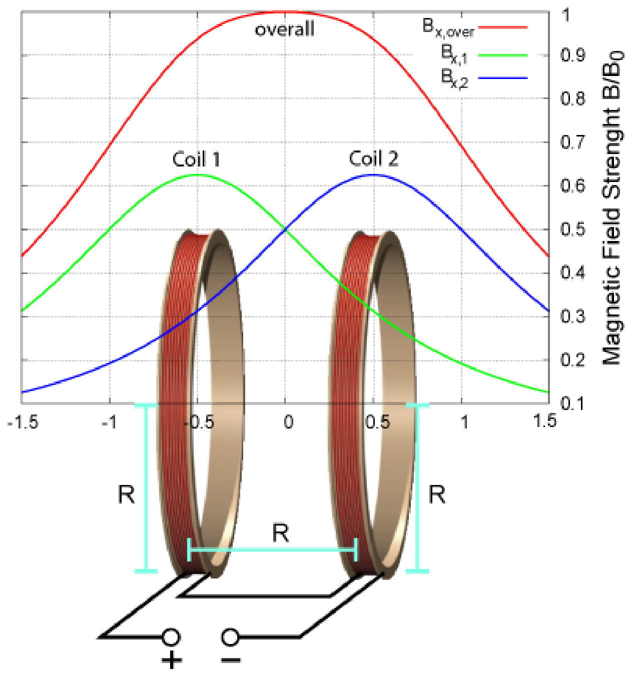

Figure 9: Example of a Helmholtz coil pair, by adding up the magnetic fields of the two coils, an almost homogeneous magnetic field is generated inside of the pair [2].

The PACMAG has been used to generate a magnetic field. The PACMAG device comprises three pairs of Helmholtz coils, two coils in each direction, owned by the Surgical Robotics Laboratory. Each pair of coils can generate an almost completely homogeneous magnetic field in one of the three dimensions, X, Y, and Z. Fig. 9 shows an example of a pair of Helmholtz coils.

In a previous study by a bachelor student at the University of Twente, Gauss meter experiments were performed on the PACMAG to test the magnetic field generated by the Helmholtz coils. The experiments showed minor differences between the set magnetic field in the machine's code and the actual magnetic field measured with a Gauss meter when going above 42 mT [14]. For this reason, the range of the experiment has been set from -40 mT to 40 mT, using increments of 1 mT.

Warm water is used to bring the sample above the glass transition temperature. To be able to do this, a waterproof container has been designed. The container also has a few other requirements; namely, it has to fit within the operating space of the PACMAG while not limiting the range of the L-shape sample. Next, it has to be see-through so cameras can measure the bending angles. Lastly, it is desired to be able to attach the sample to the container easily so it can be easily reached when changes need to be made to the sample.

Plexiglass has been chosen as the material for the container as it is easy to make using a laser cutter, and it is see-through. The container is 50 mm high, 100 mm long, and 60 mm wide. Fig. 10 shows the finished container with a sample fixed in a clamping mechanism. The clamping mechanism is made out of 2 small plates. Both plates have tapped holes so the plates can be screwed together with the sample clamped between them. The clamper can be removed and replaced from the container as one side is clamped inside a slot on the inside of the container. Fig. 11 shows the clamper and the slot it can be placed into. Appendix A.2 shows a more detailed explanation of the design of the container.

The last part of the setup is the placement of the cameras. As mentioned earlier, two cameras are required to measure both bending angles. Fig. 12 shows the top view of the container with the sample and where the cameras are placed. Fig. 13 shows photos from experiment 1 with no magnetic field applied.

Three experiments have been performed with different magnetic field directions and magnet placement. Table 3 shows the choices made for each experiment. For each experiment, the water temperature has been kept between 44°C and 35°C because this is high above the glass transition temperature and close to human body temperatures. Furthermore, 81 sets of photos have been made for all experiments, including a front and side view with the magnetic field strength ranging from -40 mT to 40 mT with steps of 1 mT. These

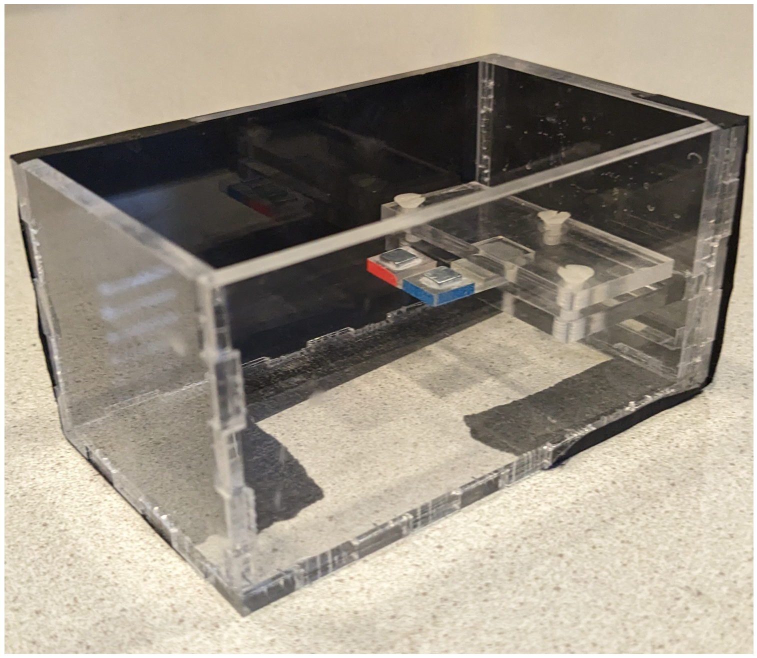

Figure 10: The container used for the experiments to fix the sample and hold warm water to heat the sample.

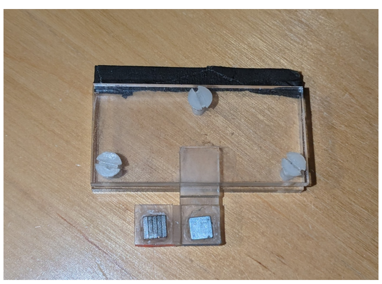

(a) Two panels to fix the sample in place by clamping it between them using three plastic screws.

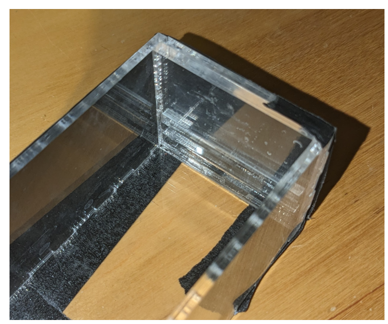

(b) Inside of the container with slots to clamp the clamping panels in.

Figure 11: Close-up photos of the mechanism used to fix the sample in the container.

pictures will be processed to determine the bending angles for all three Experiments.

3.3 Processing

Once the experiments have been done, the photos can be used to determine bending angles. It has been decided to automate the process of measuring the bending angles, as this is a more accurate way to measure, plus it is faster than doing it by hand.

To do this, the image processing toolbox of Matlab has been used. The angles can be estimated quite accurately by determining all pixels in the photo that show the side of the panels. The image processing toolbox can determine this by filtering out different colours. For this reason, the sides of the panels have been coloured using coloured tape, as can be seen in Fig. 13. Fig. 14 shows an example of a filter created to select the pixels showing the red-coloured panel side. A reflection of the panel can be seen on the surface of the water. This is not desired, but it can easily be removed by cropping the photo.

Once the filter has been applied to the photo, the coordinates of the selected pixels are saved. From these pixels, the outliers are removed using a standard Matlab function. Once the coordinates of the side of the

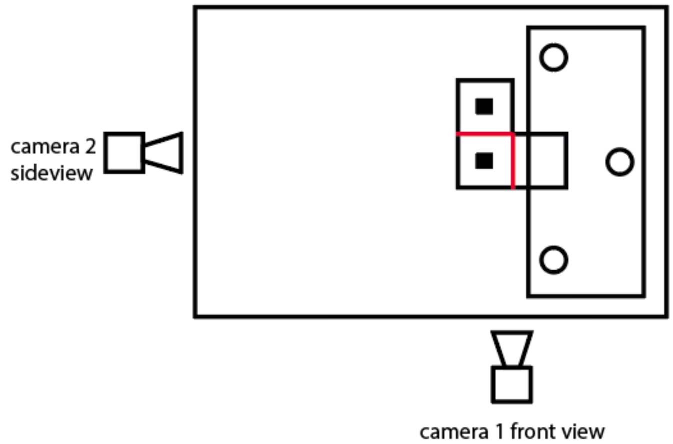

Figure 12: A top view of the container with a sample inside and showing the camera placement.

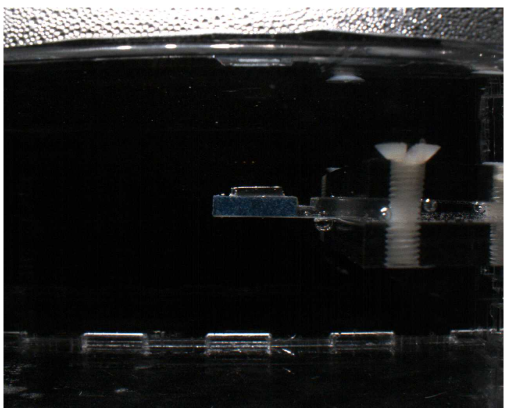

(a) Frontview.

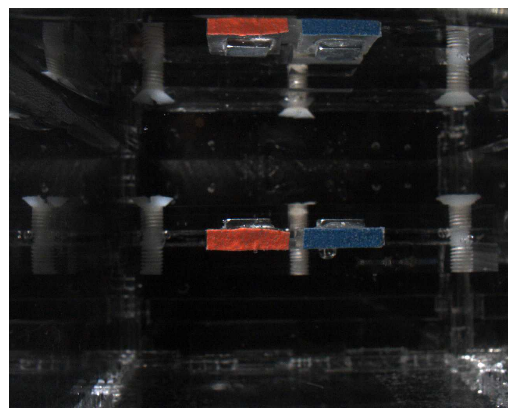

(b) Sideview.

Figure 13: Photos taken from experiment 1 with magnetic field strength 0 mT.

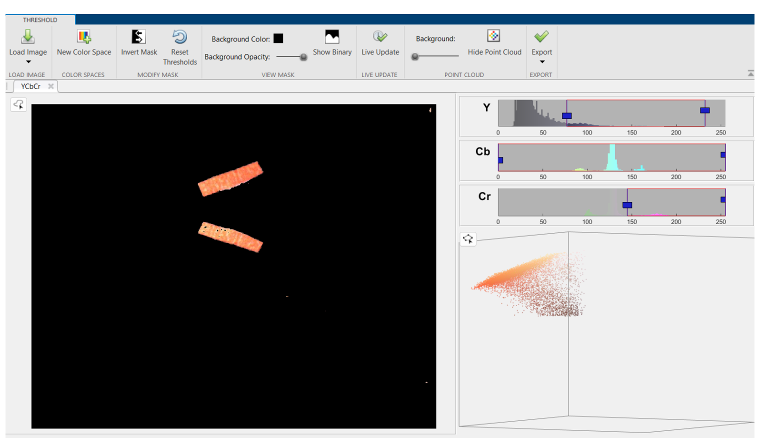

Figure 14: Experiment photo with a filter applied to locate the side of the second panel.

Table 3: The settings chosen for each of the three experiments.

Experiment	Magnetic field direction ($\vec{B^0}$)	Dipole moment 1 direction ($\vec{m_1^1}$)	Dipole moment 2 direction ($\vec{m_2^2}$)
1	(0,-1,0)	(0,0,1)	(0,0,1)
2	(-1,0,0)	-	(0,0,1)
3	(-1,-1,0)	(0,0,1)	(0,0,1)

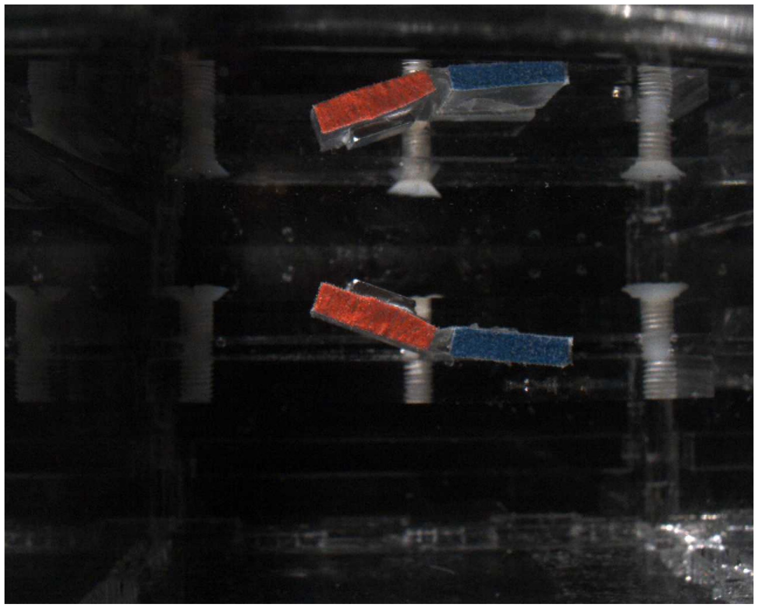

Figure 15: Photo from experiment 2 with a magnetic field strength of 37 mT.

panel have been selected, a linear line is fitted through the coordinates using the Matlab fitting tool. From the slope of this line, the angle can be calculated. This has been done for each picture and each side of the panels.

An unexpected extra bending angle started to show while a magnetic field was applied in the Y direction. As seen in Fig. 15, the first penal started to twist around the hinge, the side of the panel marked with blue. Meaning that this angle has to be measured as well.

When a bending occurs at both hinges, the angles seen in the side view are no longer entirely accurate. Only a projection of α_2 can be measured. This is because the panels rotate out of the screen, with the angle α_1. A calculation for this projection has to be made to determine the actual angles from the measured angles.

In Fig. 16, a sketch is made of the projection of the bending angle. Table 4 explains the names corresponding to the sketch. The sketch consists of 4 different triangles. All with one corner of 90°. Using geometrics Eqns. (21)-(22)-(23) can derived from this Fig. 16. Combining these equations gives Eqn. (24). Since α_1 and α_2' are measured using the image processing tool α_2 can be calculated using Eqn. (24).

$$\sin(\alpha_2') * L' = \cos(\alpha_1) * d. \tag{21}$$

$$d = \sin(\alpha_2) * L. \tag{22}$$

$$\cos(\alpha_2') * L' = \cos(\alpha_2) * L. \tag{23}$$

$$\tan(\alpha_2') \sec(\alpha_1) = \tan(\alpha_2). \tag{24}$$

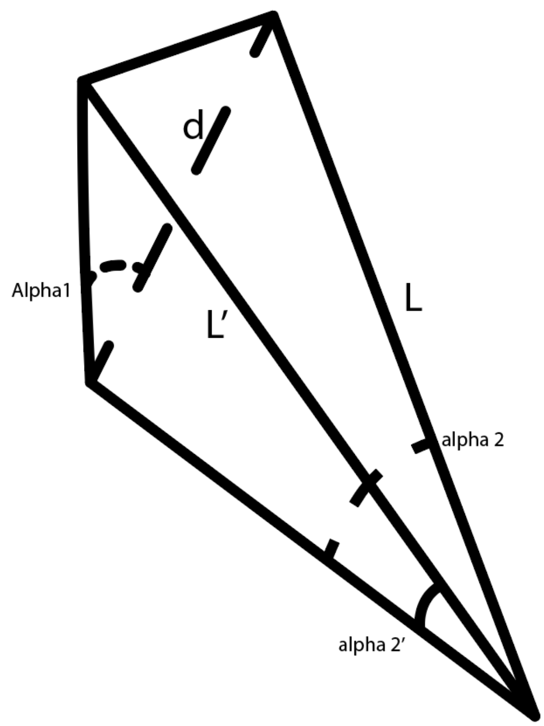

Figure 16: A sketch of the orientation of the panel side seen under an angle. Table 4 explains the symbols used in the figure.

Table 4: An explanation of all components in the sketch of Fig. 16.

Symbol in figure	Description
Alpha 1	The bending angle of the first hinge as described in the theory
Alpha 2	The bending angle of the second hinge as described in the theory
Alpha 2'	The bending angle of the second hinge as measured with the camera
L	The length of the side of the panel
L'	The length of the side of the panel as measured on the camera
d	An arbitrary length used in the geometry of the sketch to determine the final angles

4 Results

In this section, the processed results of the experiments performed are shown. Some photos taken during the experiments are included in Appendix A.3. These photos include photos from a failed experiment.

4.1 Experiment 1

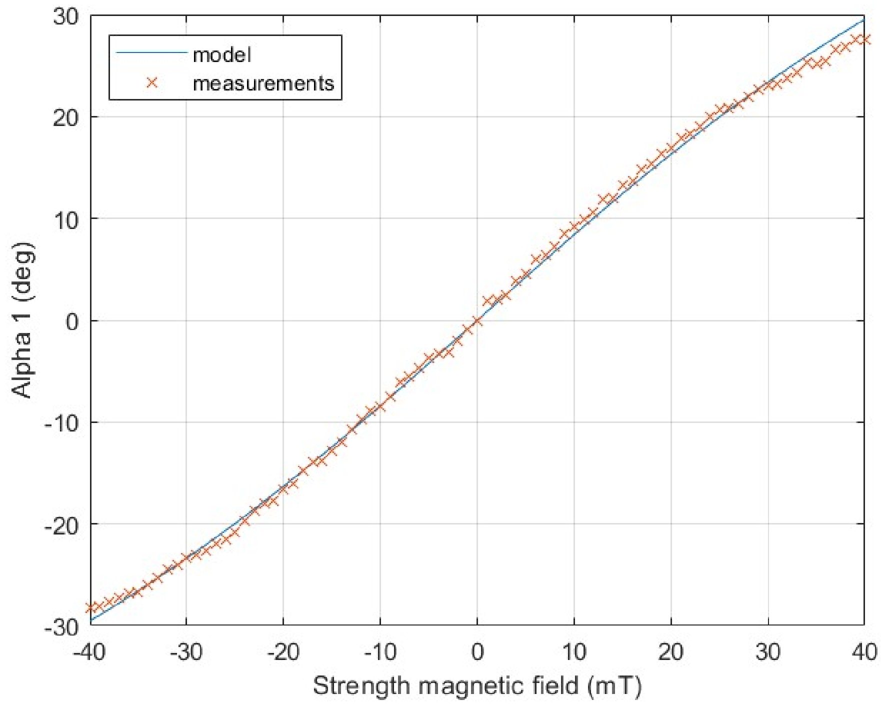

Figure 17: Results of the first experiment, as described in Table 3. Compared with the model with an estimated spring constant $K = 0{,}27$ Nm/rad.

Fig. 17 Shows the first experiment's results as described in Table 3. During this experiment, no bending has been measured at the second hinge, which is as expected when inspecting the model, Fig. 4b. By comparing the experiment's results with the model, a value for the spring constant of the hinges has been estimated to be around $K \approx 0{,}27$ Nm/rad. This value has been used for the model predictions in Fig. 17.

4.2 Experiment 2

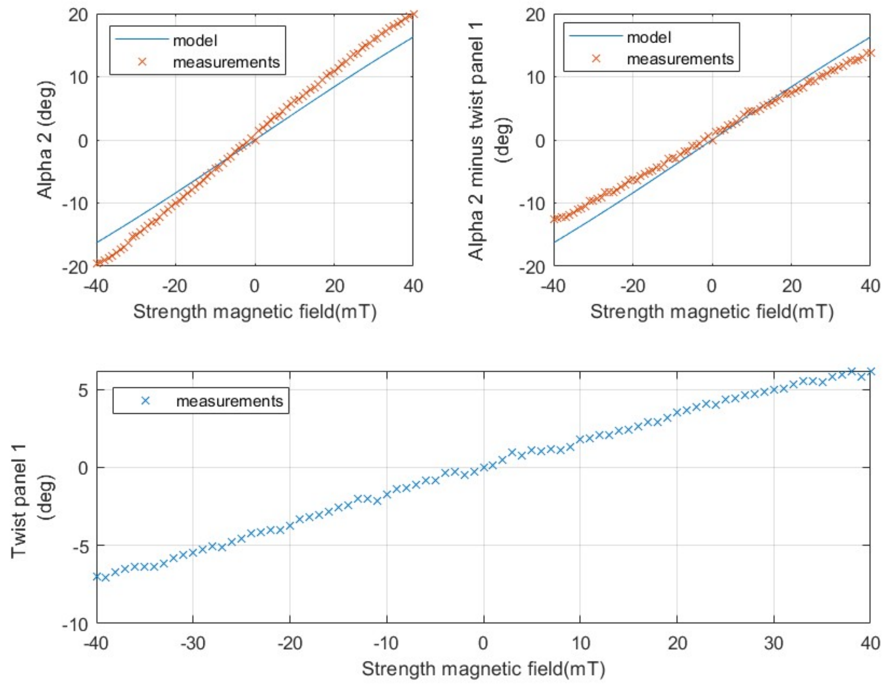

Figure 18: Results of the second experiment, as described in Table 3. Compared with the model with $K = 0{,}27$ Nm/rad.

Fig. 18 shows the results of the second experiment. During this experiment, a twist around the first hinge was measured. This has been plotted at the bottom of the figure. The top left plot shows the second bending angle α_2 measured to the horizon. The top right plot shows the same angle, but measured to the first panel, the difference between the twist of panel one and the second bending angle.

The model expectation has been included in the top two plots, using the value $K = 0{,}27$ Nm/rad as approached with the results of experiment 1. In this experiment, no bending has been measured at the first hinge. This is expected when inspecting the model; see Fig. 4c.

4.3 Experiment 3

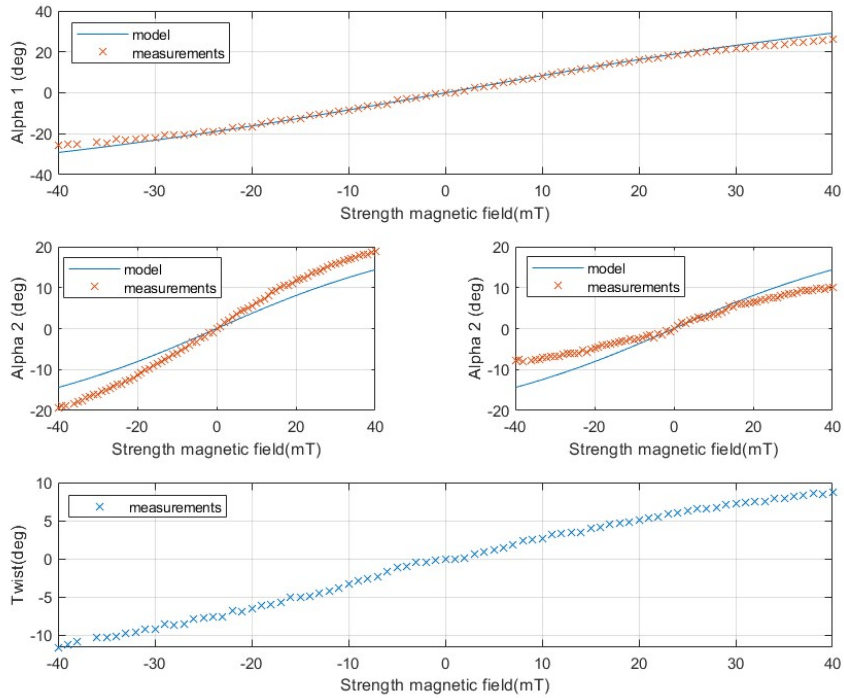

Figure 19: Results of the third experiment, as described in Table 3. Compared with the model with $K = 0{,}27$ Nm/rad.

Fig. 19 Shows the results of the third experiment compared with the model using the spring constant $k = 0{,}27$ Nm/rad. The top plot shows the bending angle of the first hinge, α_1, together with the model expectation of this angle. The middle two plots show the second bending angle, α_2, the left plot shows the results measured to the horizon, and the right plot shows the bending angle measured to the first panel. Lastly, the plot at the bottom shows the twist around the first hinge measured.

5 Discussion

This discussion is divided into four sections—discussing the first, second, and third experiments and the materials and methods.

5.1 Experiment 1

The results of the first experiment seem to be as expected. The sample only bends at the first hinge. As shown in Fig. 17, the curve of bending angles has an S-shape, just as expected from the model. After estimating a value for the spring constant for the hinges, the estimation curves seem to be very close to the results.

Nonetheless, when inspecting the results very closely, the results seem to show a slight deviation from the expectation when going above 20°, but not when going below -20°. This could be because the top edges of the hinge are starting to get compressed together, which could change the behaviour of the rotational spring.

However, no clear conclusion can be drawn about this deviation from the current results. This is because the deviation is minimal and could be interpreted as a measuring error. To be more confident about this, a more extensive range of bending of α_1 could be inspected to see if there's a clear difference in two directions of the bending angle.

If there is a difference, it might not be accurate enough to model the hinge with a rotational spring constant. An investigation would have to be done to determine the bending angle range for which a linear approximation would still hold. This range must be considered when designing a controllable tool using magnetic actuation of a 3d shape memory origami structure.

5.2 Experiment 2

When inspecting the results of the second experiment, a few things can be discussed. First, when looking at the shape of the curve of the measured bending angles, it seems to behave like the S-shape as expected from its model. However, a big issue is the introduction of the twist of the first panel around its hinge when inducing a torque on the magnet in the Y direction.

This panel bending was unexpected, and since this twist angle reaches about 7°, it is not negligible. This means the assumption of bending only happening in one direction for each hinge made in section 2.3 is false. This makes the model not accurate enough.

The model would have to be updated on this by including the twisting in it. This can be done by introducing a new angle and formulating another equilibrium equation for each hinge with the direction corresponding to this hinge. This would be the Y direction for the first hinge and the X direction for the second hinge.

Furthermore, the bending angle α_2 seems to deviate from its expectation, even when subtracting the twist angle from it. Two reasons could explain this. The first reason is that the spring constant of this second hinge could differ from that of the first hinge. They both have a thickness of approximately 1 mm. However, creating these hinges by engraving them with a laser cutter is not a super accurate method. As the material tends to melt while engraving.

Another reason for this could be the twist induced at the first hinge. Because of this twisting, the dipole moment of the magnet is already closer to being aligned with the magnetic field lines. This would make the angle between these two vectors smaller, reducing the torque induced by the magnetic field on the magnet. Making the bending angle around the hinge smaller.

5.3 Experiment 3

When inspecting the results of experiment three, it seems like the expectation of the first bending angle is fairly accurate. However, like in the second experiment, a twist around the first hinge is introduced, and the second hinge expectation seems to deviate from the measured angles.

Next, the angles measured at a magnetic field strength of -37mT are missing. They're missing because a mistake was made when storing the photos of this measurement.

5.4 Materials and Methods

The first discussion point is using a different material than initially intended. The initial intention was to use the Material SMP DiAPLEX. However, it was very tough to produce clean sheets of this SMP. All sheets made were full of bubbles and were not useable for the experiment because these inconsistencies in their structure could significantly influence the origami structures' mechanical properties. Also see Appendix A.1.

Because of the production issues, a different material, Norland Optical Adhesive 63, has been chosen. This material is also an SMP with a low glass transition temperature, which is desired for this research. However, this material is more brittle than the SMP DiAPLEX. This causes it to tear faster, which limits the hinge's bending range.

In the experiments, the samples are bending from -30°to 30°. It would have been interesting to investigate a larger range of bending. This could have been done by using stronger or more magnets. However, Since the material is more brittle than the DiAPLEX, the material started to tear at larger angles; examples of this are included in the appendix A.3. This would decrease the shape memory effect and change the sample's behaviour.

6 Conclusions and Future Work

This study has focused on the experimental evaluation of magnetic actuation of a 3D-shaped memory origami structure and whether it is possible to predict its behaviour. An L-shape with three panels has been investigated by making a basic model and comparing it with three experiments.

From the findings of this thesis, it can be concluded that when applying torques in 3 dimensions on a shape memory origami structure, bending at the hinges might occur in more than one direction, which means that the model is not accurate enough to predict the behaviour of the L-shape memory origami structure. A subsequent study could focus on this twisting behaviour.

Another issue has been the material of the shape memory origami structures. The material used in this study was too brittle to investigate an excellent bending range of the origami structures. Another point of attention for the following studies could be the material. An SMP that is more flexible and easier to manufacture could be investigated, or a focus could be put on improving the manufacturing technique of sheets of SMP DiAPLEX.

References

[1] M. Behl and A. Lendlein, "Shape-memory polymers," *Materials Today*, vol. 10, no. 4, pp. 20–28, 2007. [Online]. Available: https://www.sciencedirect.com/science/article/pii/S1369702107700470

[2] "Magnetic field of two helmholtz coils." [Online]. Available: https://virtuelle-experimente.de/en/b-feld/b-feld/helmholtzspulenpaar.php

[3] G. P. Dobson, "Trauma of major surgery: A global problem that is not going away," *International Journal of Surgery*, vol. 81, p. 47–54, 2020.

[4] F. Leong, N. Garbin, C. D. Natali, A. Mohammadi, D. Thiruchelvam, D. Oetomo, and P. Valdastri, "Magnetic surgical instruments for robotic abdominal surgery," *IEEE Reviews in Biomedical Engineering*, vol. 9, p. 66–78, 2016.

[5] M. Tonutti, D. S. Elson, G.-Z. Yang, A. W. Darzi, and M. H. Sodergren, "The role of technology in minimally invasive surgery: State of the art, recent developments and future directions," *Postgraduate Medical Journal*, vol. 93, no. 1097, p. 159–167, 2016.

[6] I. Alkatout, U. Mechler, L. Mettler, J. Pape, N. Maass, M. Biebl, G. Gitas, A. S. Laganà, and D. Freytag, "The development of laparoscopy—a historical overview," *Frontiers in Surgery*, vol. 8, 2021.

[7] J. Delaey, P. Dubruel, and S. Van Vlierberghe, "Shape-memory polymers for biomedical applications," *Advanced Functional Materials*, vol. 30, no. 44, p. 1909047, 2020.

[8] D. L. Safranski and J. C. Griffis, *Shape memory polymer device design.* William Andrew, 2017.

[9] A. R. Ahmed, O. C. Gauntlett, and G. Camci-Unal, "Origami-inspired approaches for biomedical applications," *ACS Omega*, vol. 6, no. 1, p. 46–54, 2020.

[10] M. Johnson, Y. Chen, S. Hovet, S. Xu, B. Wood, H. Ren, J. Tokuda, and Z. T. Tse, "Fabricating biomedical origami: A state-of-the-art review," *International Journal of Computer Assisted Radiology and Surgery*, vol. 12, no. 11, p. 2023–2032, 2017.

[11] N. Ebrahimi, C. Bi, D. J. Cappelleri, G. Ciuti, A. T. Conn, D. Faivre, N. Habibi, A. Hošovský, V. Iacovacci, I. S. Khalil, and et al., "Magnetic actuation methods in bio/soft robotics," *Advanced Functional Materials*, vol. 31, no. 11, p. 2005137, 2020.

[12] D. Jordan, "State of the art in magnetic resonance imaging," *Physics Today*, vol. 73, no. 2, pp. 34–40, 02 2020. [Online]. Available: https://doi.org/10.1063/PT.3.4408

[13] S. V. Cox, "Optimisation of origami structures for magnetic actuation in minimally invasive surgery," 2022.

[14] Q. Helm, "Development of a shape memory polymer-based zigzag structure by magnetic actuation," 2022.

[15] "Shape memory polymer, smp technologies inc., diaplex," 2023. [Online]. Available: http://www2.smptechno.com/en/smp/

[16] "Norland optical adhesive 63." [Online]. Available: https://www.norlandprod.com/adhesives/noa%2063.html

A Appendix

A.1 Production of Sheets of SMP DiAPLEX

Multiple Attempts have been made to produce a sheet SMP DiAPLEX to make an L-shaped Origami structure. Fig. A.1 shows a few results of attempts to make these sheets. However, none of the attempts have been successful.

DiAPLEX is a two-component SMP consisting of resin A and hardener B. These two components must be mixed, put in a mold to get the desired shape, and put in the oven to cure the material. The following steps have been followed to try to make a SMP sheet:

1. Put an equal amount of resin A and hardener B into the two chambers of the two-component glue mixer.
2. Seal the backside of the two chambers of the glue mixer, remove the cap at the tip of the glue mixer, and put it with its tip upwards in a vacuum chamber for 2 hours to remove all bubbles from the resin and hardener.
3. Make a mold out of plexiglass; make sure to put a sheet of silicon between the top and bottom plate. This way, the material won't stick to the mold. Also, glue down the silicon sheet to the bottom of the mold to avoid bubbles growing underneath the silicon sheet.
4. Make sure the mold is dust and grease-free.
5. After all bubbles have been vacuumed out of solutions A and B, push the solutions upwards in the chambers, pushing out the air while not shaking or rotating the solutions.
6. When almost all air is pushed out, attach the mixing tip to the tip of the glue mixer gun.
7. Rotate the glue mixer gun, pointing the tip downwards. Push the solutions through the mixing tip and pour them into the mold. (Do not use the first and last parts coming out of the glue gun because these might contain a lot of bubbles).
8. When filled, put the mold quickly but carefully in the vacuum chamber for max 2 minutes to remove some of the little bubbles that formed in the mold.
9. Finally, put the mold in the oven to cure for 2 hours at 70°C.
10. When finished, it can be removed from the mold by laser cutting the edges.

As a first attempt, the mold has been made in the desired final L-shape see Fig. A.1c. In later attempts, it was decided to make one bigger sheet, Fig. A.1a and Fig. A.1b, and try to laser cut the L-shape out of this sheet. However, a bigger and rectangular shape did not have less bubble formation.

(a) Example attempt 1.

(b) Example attempt 2.

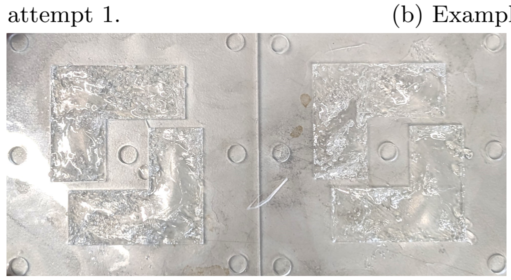

(c) Example attempt 3.

Figure A.1: The three figures above show different SMP DiAPLEX sheets with bubbles grown in the material.

A.2 Design Details of the Experiment Container

Table A.1 shows the experiment container's dimensions. The parts of the container have been designed and put together in Solidworks. Fig. A.2 shows a final result in Solid works. Figs. A.3 and A.4 show all parts of the experiment container. Fig.A.3 shows all parts with a thickness of 3mm and Fig.A.4 shows the parts having a thickness of 4mm.

All parts have been cut out using a laser cutter. Once done, the container's bottom and all four sides have been glued together using watertight glue. Once tested to determine whether it is waterproof, the plate to attach the clamper to has been glued to the short side of the container. Finally, the holes of the clamper top and bottom have been tapped so they can be screwed together using plastic screws.

Table A.1: Dimension of the experiment container.

Dimension	Value (mm)
Height	50
Length	100
Width	60
Thickness outside container	3
Top plate clamper	50 by 24 by 3
Bottom plate clamper	50 by 30 by 4
Clamper attaching plate	54 by 47 by 4
Heights clamper attaching slots	5 and 15
Clamping screws diameter	3

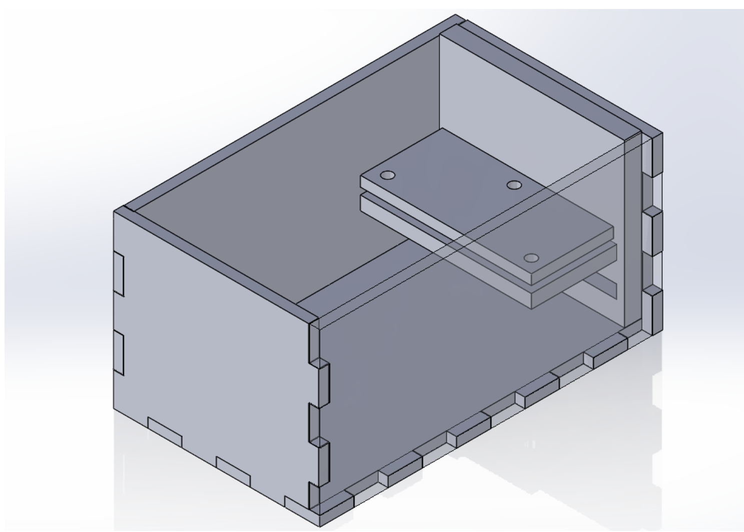

Figure A.2: Assembly of the experiment container made in Solidworks.

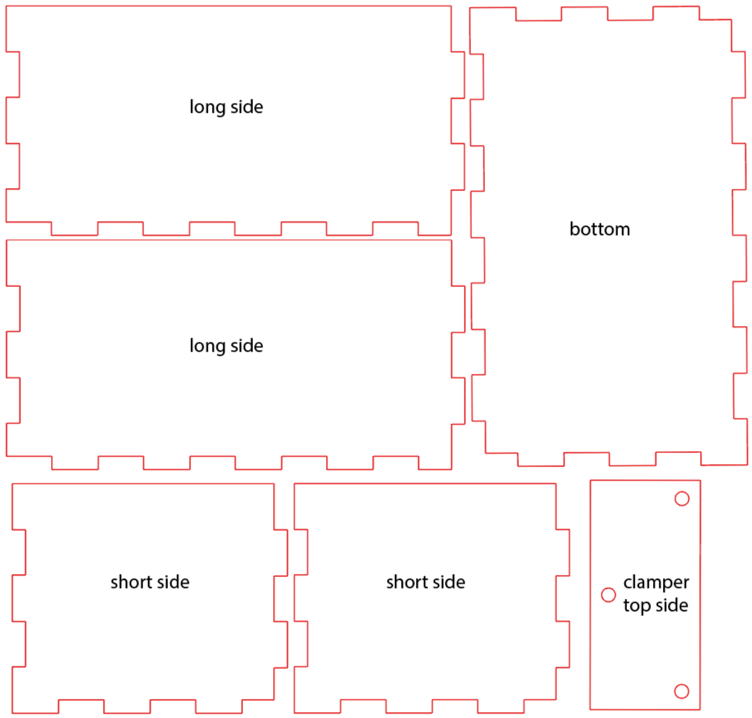

Figure A.3: Cutout of the bottom and sides of the container and the top plate of the clamping mechanism. With a plate thickness of 3 mm

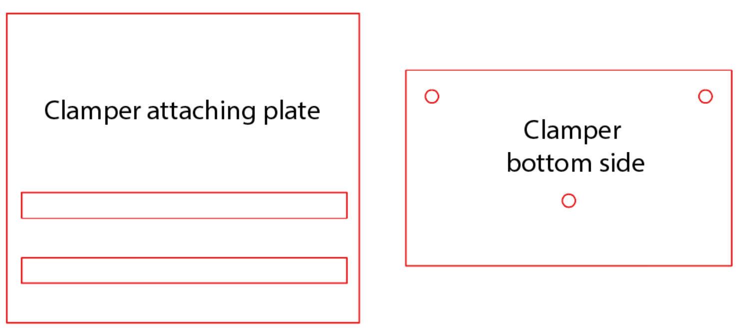

Figure A.4: Cutout of the bottom plate of the clamping mechanism together with the side in which the clamping mechanics can be attached. With a plate thickness of 4 mm.

A.3 Experiment Photos

In this appendix photos from the experiments have been included. Each experiment's front and side views with the magnetic field strengths of -40 mT, -20 mT, 20 mT, and 40 mT have been included. Fig. A.5 shows photos from experiment one, Fig. A.6 shows photos from experiment two, and Fig. A.7 shows photos from experiment three

Fig. A.8 shows photos from a failed experiment. In this experiment, the hinge of the sample started to tear, making the results unusable. This failure occurred because stresses on the material hinges were too high due to the material's brittleness.

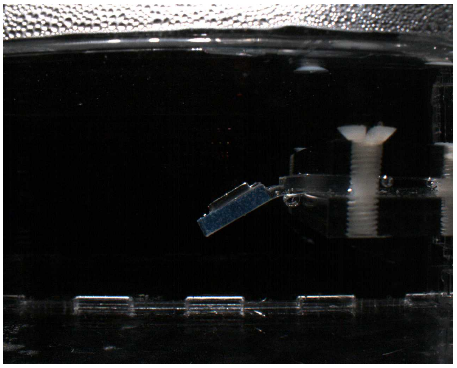

(a) Front view -40 mT.

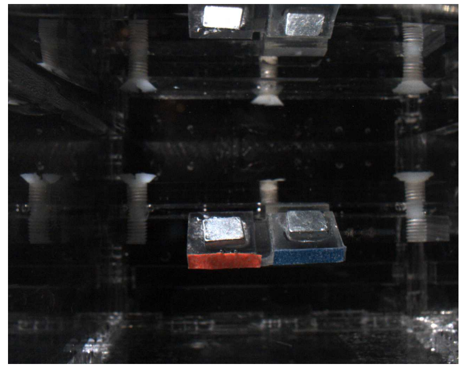

(b) Side view -40 mT.

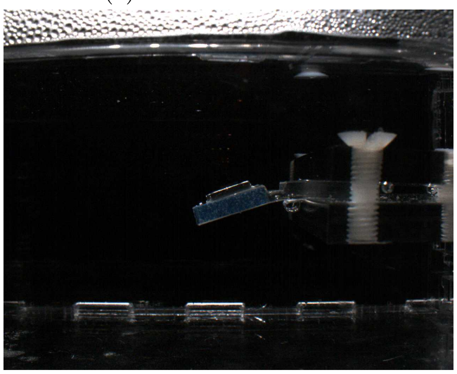

(c) Front view -20 mT.

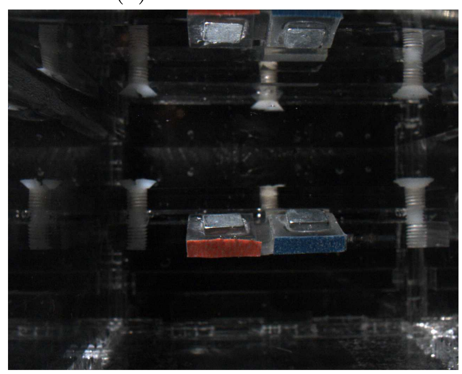

(d) Side view -20 mT.

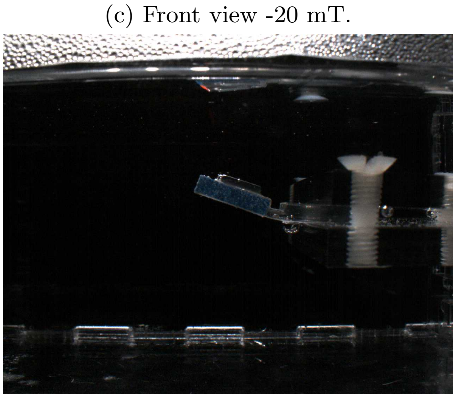

(e) Front view 20 mT.

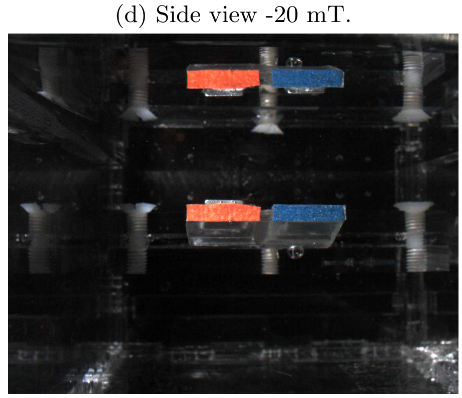

(f) Side view 20 mT.

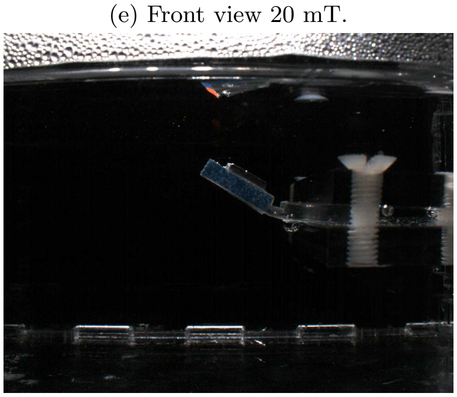

(g) Front view 40 mT.

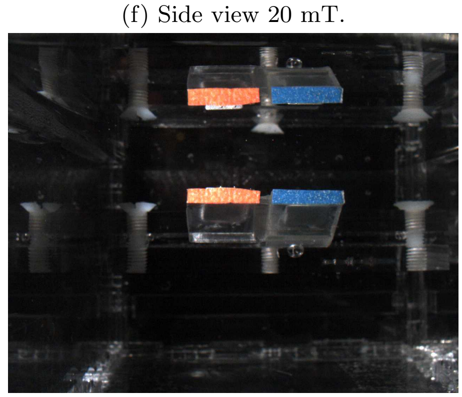

(h) Side view 40 mT.

Figure A.5: Photos taken from the first experiment.

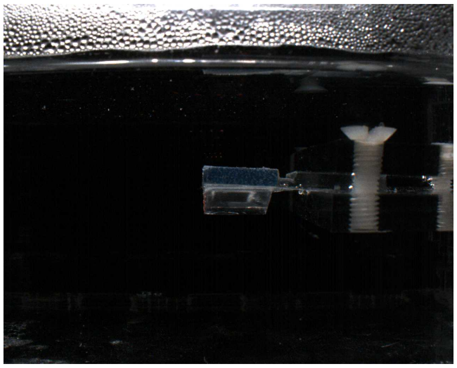

(a) Front view -40 mT.

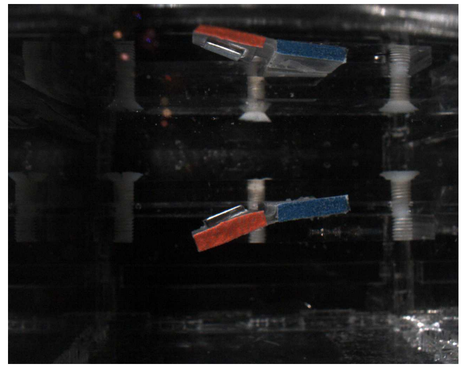

(b) Side view -40 mT.

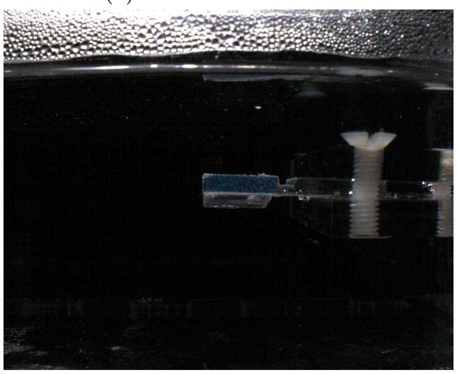

(c) Front view -20 mT.

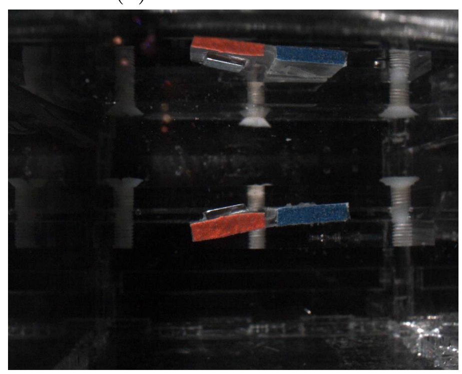

(d) Side view -20 mT.

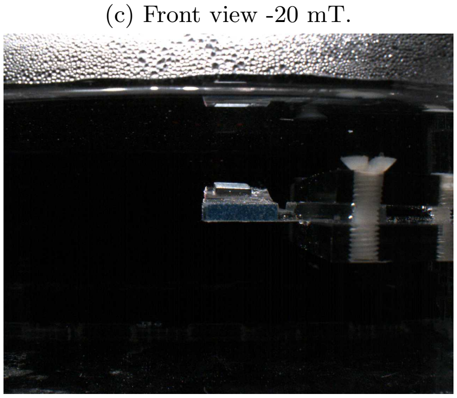

(e) Front view 20 mT.

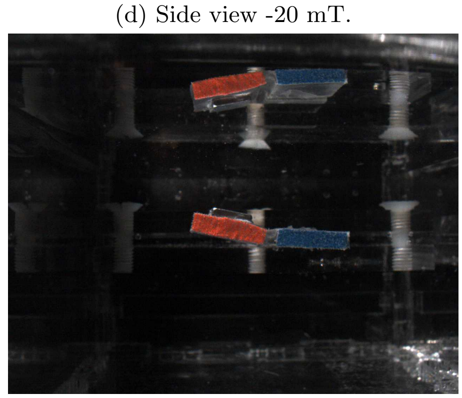

(f) Side view 20 mT.

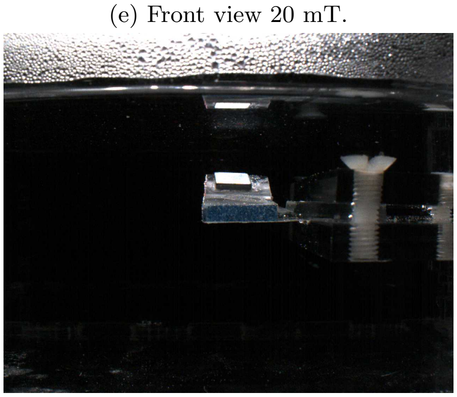

(g) Front view 40 mT.

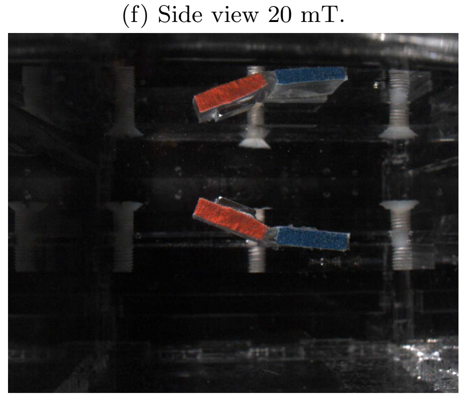

(h) Side view 40 mT.

Figure A.6: Photos taken from the second experiment.

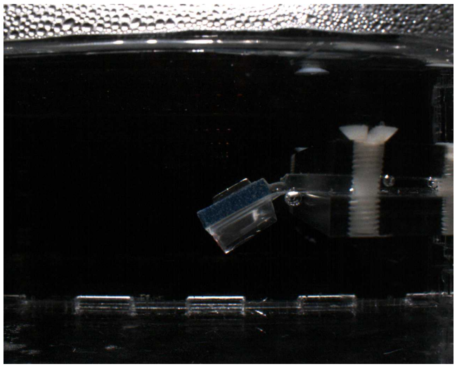

(a) Front view -40 mT.

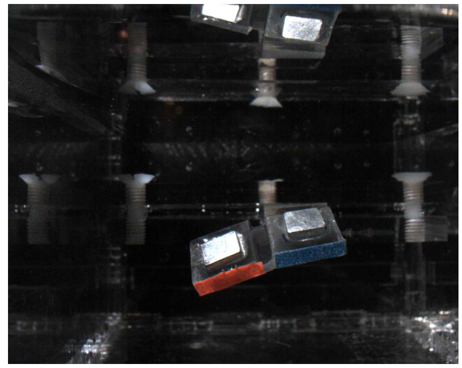

(b) Side view -40 mT.

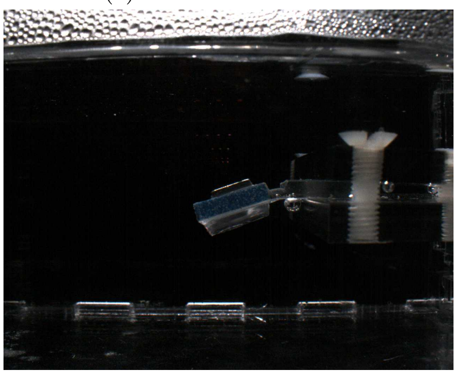

(c) Front view -20 mT.

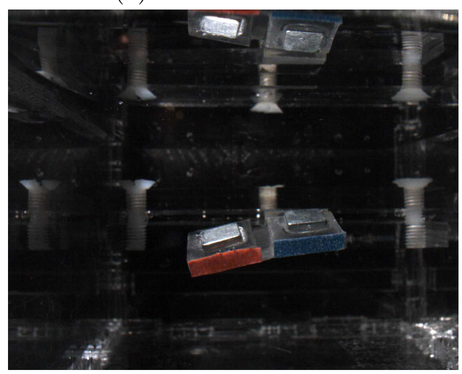

(d) Side view -20 mT.

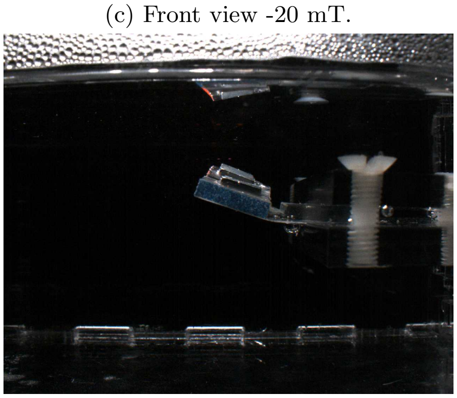

(e) Front view 20 mT.

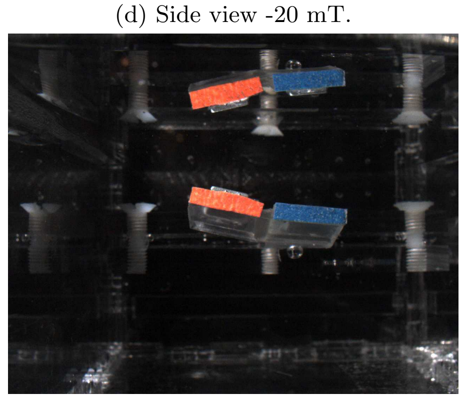

(f) Side view 20 mT.

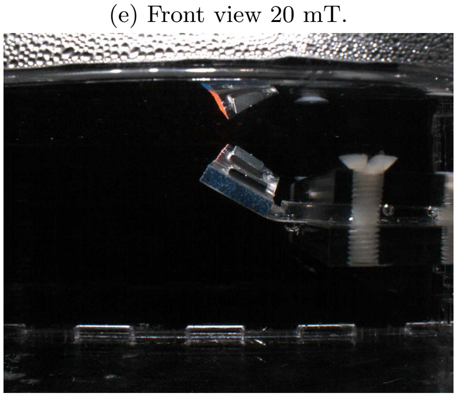

(g) Front view 40 mT.

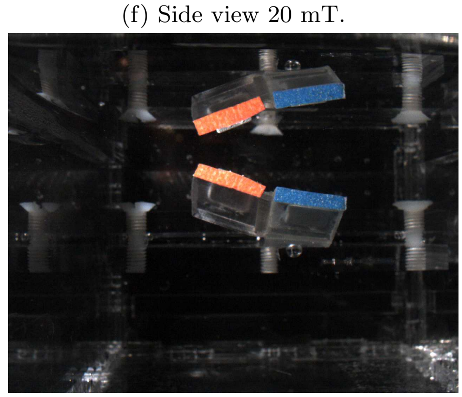

(h) Side view 40 mT.

Figure A.7: Photos taken from the third experiment.

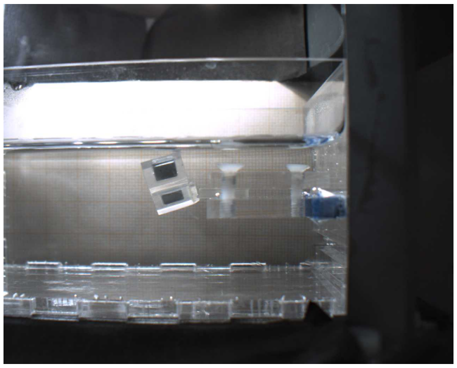

(a) Front view -30 mT.

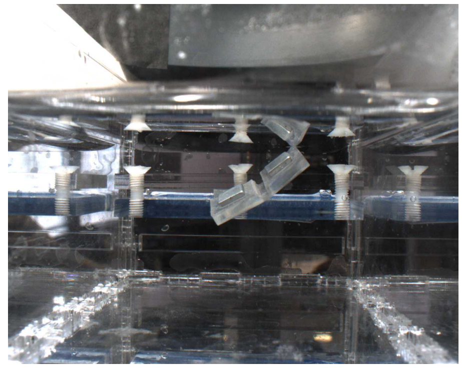

(b) Side view -30 mT.

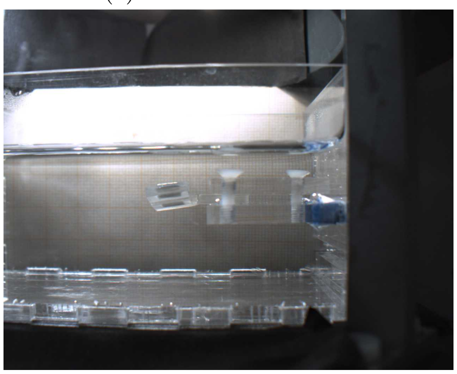

(c) Front view -15 mT.

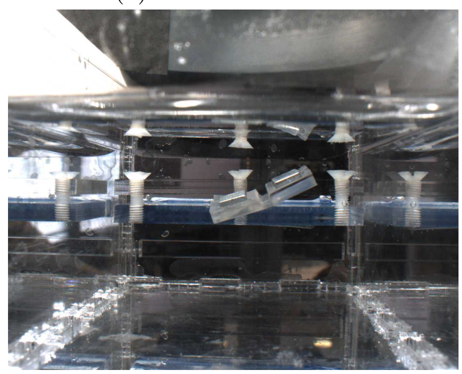

(d) Side view -15 mT.

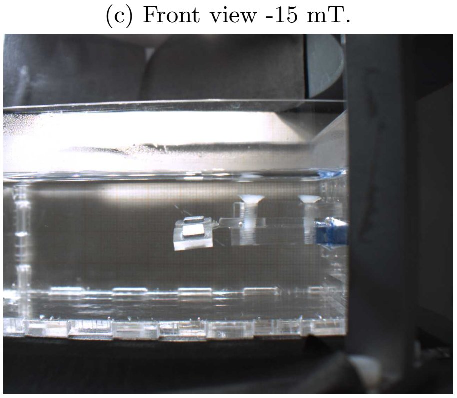

(e) Front view 15 mT.

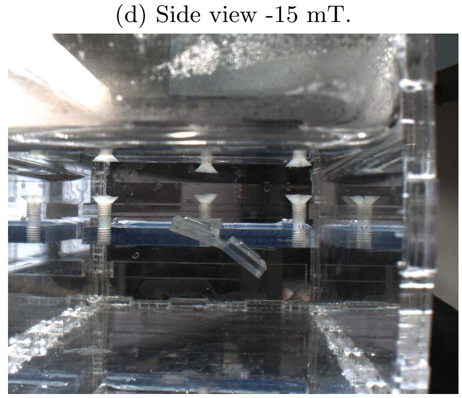

(f) Side view 15 mT.

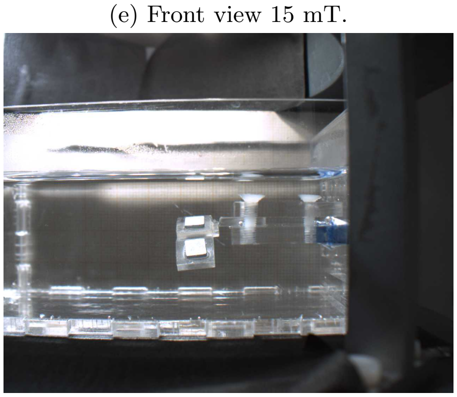

(g) Front view 30 mT.

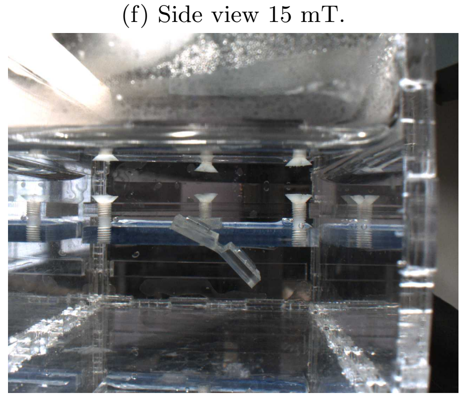

(h) Side view 30 mT.

Figure A.8: Photos taken from a failed experiment.

A Appendix

A.1 Production of Sheets of SMP DiAPLEX

Multiple Attempts have been made to produce a sheet SMP DiAPLEX to make an L-shaped Origami structure. Fig. A.1 shows a few results of attempts to make these sheets. However, none of the attempts have been successful.

DiAPLEX is a two-component SMP consisting of resin A and hardener B. These two components must be mixed, put in a mold to get the desired shape, and put in the oven to cure the material. The following steps have been followed to try to make a SMP sheet:

1. Put an equal amount of resin A and hardener B into the two chambers of the two-component glue mixer.
2. Seal the backside of the two chambers of the glue mixer, remove the cap at the tip of the glue mixer, and put it with its tip upwards in a vacuum chamber for 2 hours to remove all bubbles from the resin and hardener.
3. Make a mold out of plexiglass; make sure to put a sheet of silicon between the top and bottom plate. This way, the material won't stick to the mold. Also, glue down the silicon sheet to the bottom of the mold to avoid bubbles growing underneath the silicon sheet.
4. Make sure the mold is dust and grease-free.
5. After all bubbles have been vacuumed out of solutions A and B, push the solutions upwards in the chambers, pushing out the air while not shaking or rotating the solutions.
6. When almost all air is pushed out, attach the mixing tip to the tip of the glue mixer gun.
7. Rotate the glue mixer gun, pointing the tip downwards. Push the solutions through the mixing tip and pour them into the mold. (Do not use the first and last parts coming out of the glue gun because these might contain a lot of bubbles).
8. When filled, put the mold quickly but carefully in the vacuum chamber for max 2 minutes to remove some of the little bubbles that formed in the mold.
9. Finally, put the mold in the oven to cure for 2 hours at 70°C.
10. When finished, it can be removed from the mold by laser cutting the edges.

As a first attempt, the mold has been made in the desired final L-shape see Fig. A.1c. In later attempts, it was decided to make one bigger sheet, Fig. A.1a and Fig. A.1b, and try to laser cut the L-shape out of this sheet. However, a bigger and rectangular shape did not have less bubble formation.

(a) Example attempt 1.

(b) Example attempt 2.

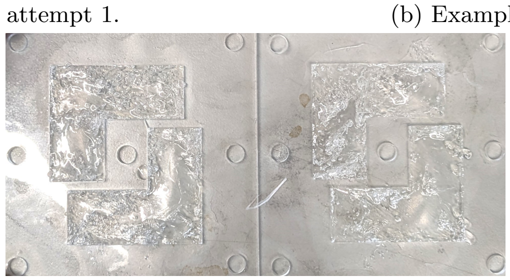

(c) Example attempt 3.

Figure A.1: The three figures above show different SMP DiAPLEX sheets with bubbles grown in the material.

A.2 Design Details of the Experiment Container

Table A.1 shows the experiment container's dimensions. The parts of the container have been designed and put together in Solidworks. Fig. A.2 shows a final result in Solid works. Figs. A.3 and A.4 show all parts of the experiment container. Fig.A.3 shows all parts with a thickness of 3mm and Fig.A.4 shows the parts having a thickness of 4mm.

All parts have been cut out using a laser cutter. Once done, the container's bottom and all four sides have been glued together using watertight glue. Once tested to determine whether it is waterproof, the plate to attach the clamper to has been glued to the short side of the container. Finally, the holes of the clamper top and bottom have been tapped so they can be screwed together using plastic screws.

Table A.1: Dimension of the experiment container.

Dimension	Value (mm)
Height	50
Length	100
Width	60
Thickness outside container	3
Top plate clamper	50 by 24 by 3
Bottom plate clamper	50 by 30 by 4
Clamper attaching plate	54 by 47 by 4
Heights clamper attaching slots	5 and 15
Clamping screws diameter	3

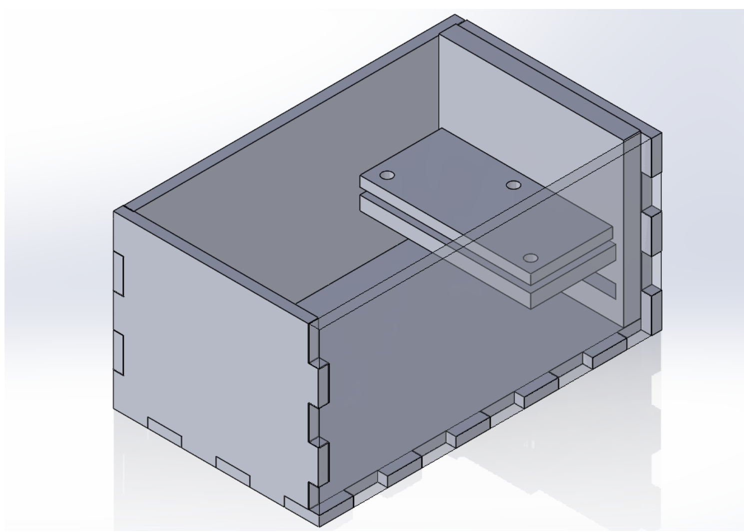

Figure A.2: Assembly of the experiment container made in Solidworks.

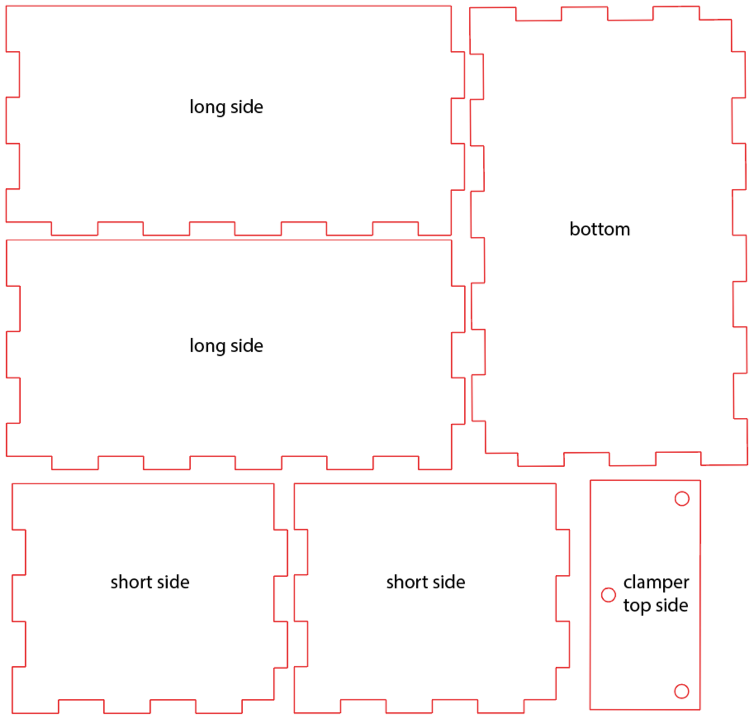

Figure A.3: Cutout of the bottom and sides of the container and the top plate of the clamping mechanism. With a plate thickness of 3 mm

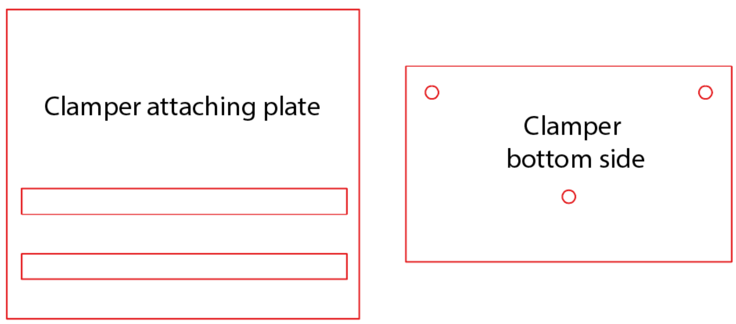

Figure A.4: Cutout of the bottom plate of the clamping mechanism together with the side in which the clamping mechanics can be attached. With a plate thickness of 4 mm.

A.3 Experiment Photos

In this appendix photos from the experiments have been included. Each experiment's front and side views with the magnetic field strengths of -40 mT, -20 mT, 20 mT, and 40 mT have been included. Fig. A.5 shows photos from experiment one, Fig. A.6 shows photos from experiment two, and Fig. A.7 shows photos from experiment three

Fig. A.8 shows photos from a failed experiment. In this experiment, the hinge of the sample started to tear, making the results unusable. This failure occurred because stresses on the material hinges were too high due to the material's brittleness.

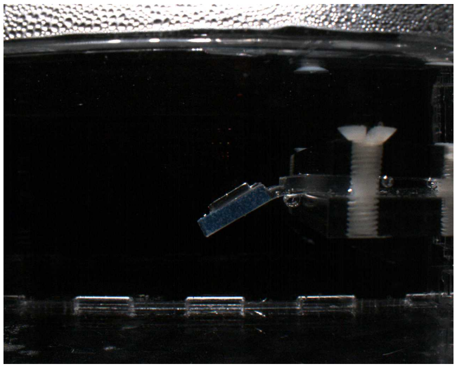

(a) Front view -40 mT.

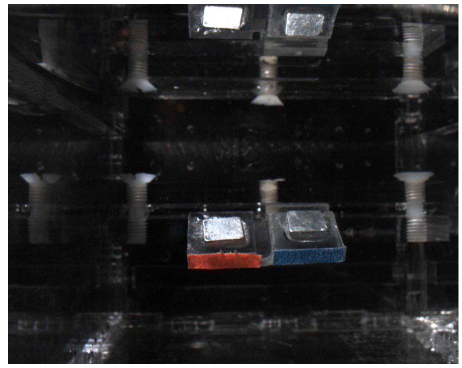

(b) Side view -40 mT.

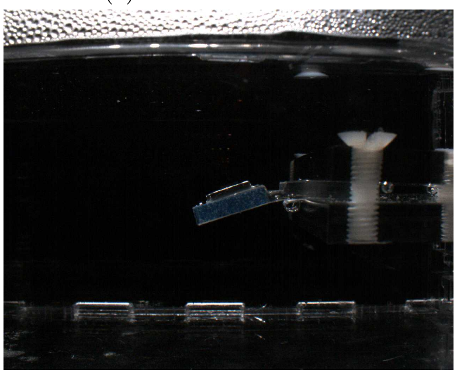

(c) Front view -20 mT.

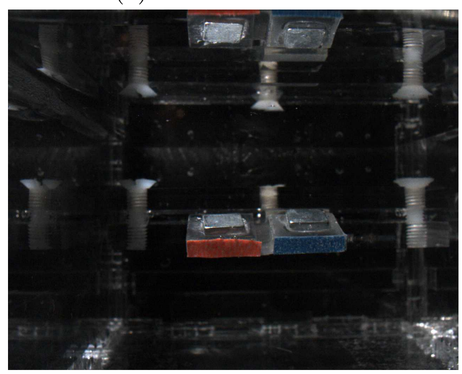

(d) Side view -20 mT.

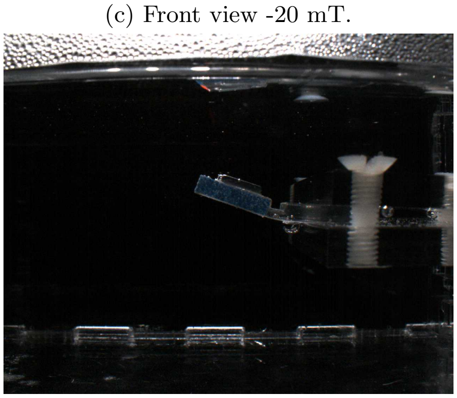

(e) Front view 20 mT.

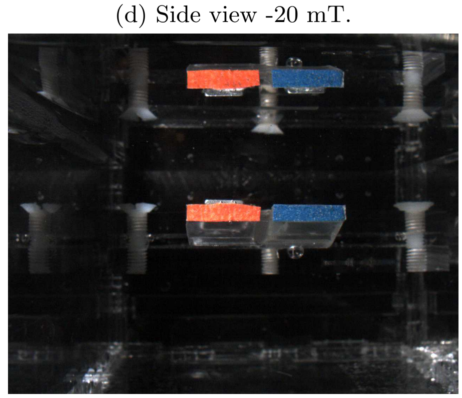

(f) Side view 20 mT.

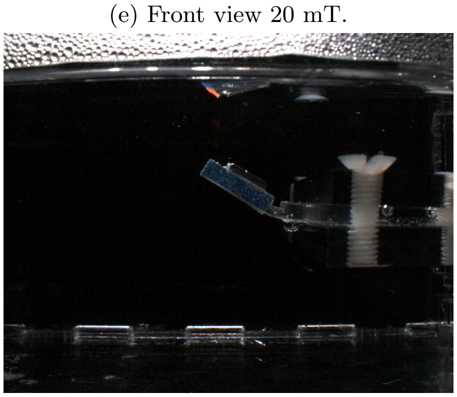

(g) Front view 40 mT.

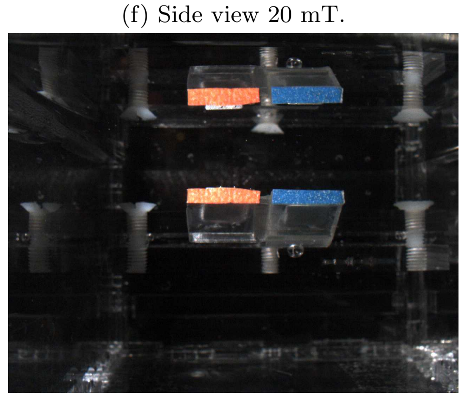

(h) Side view 40 mT.

Figure A.5: Photos taken from the first experiment.

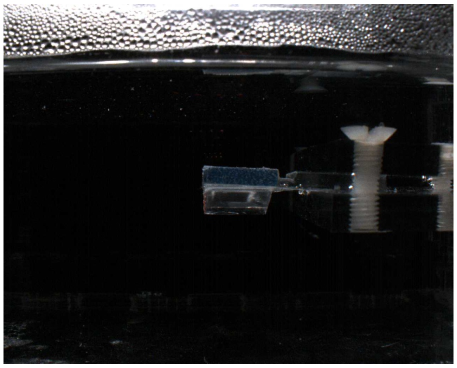

(a) Front view -40 mT.

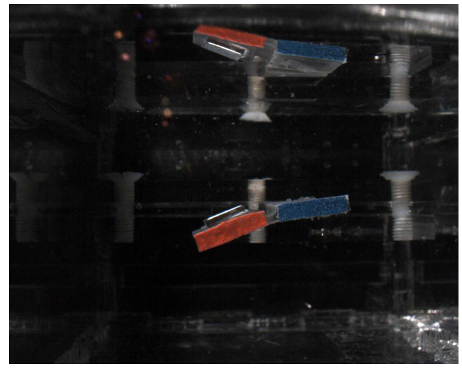

(b) Side view -40 mT.

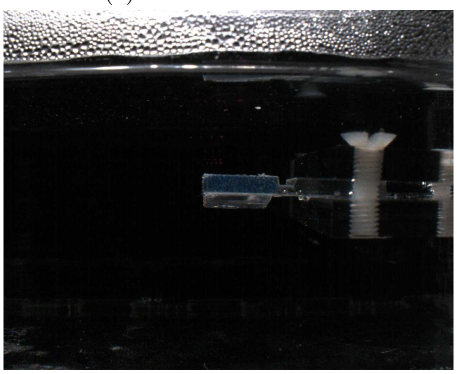

(c) Front view -20 mT.

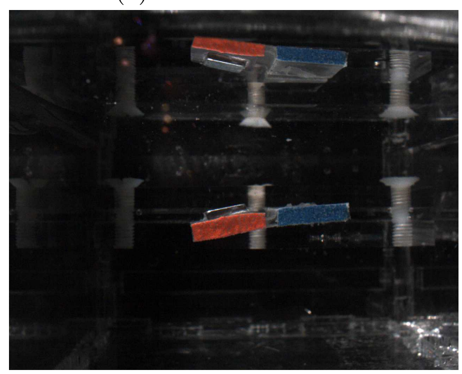

(d) Side view -20 mT.

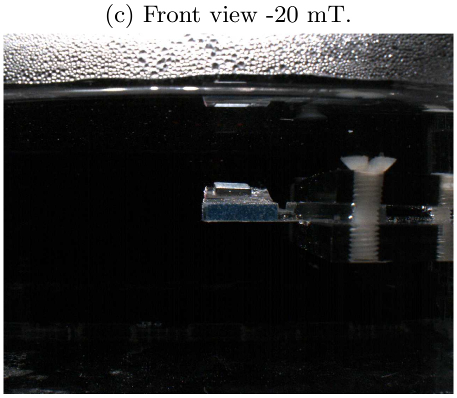

(e) Front view 20 mT.

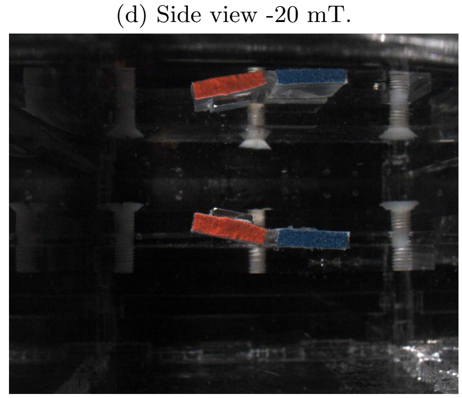

(f) Side view 20 mT.

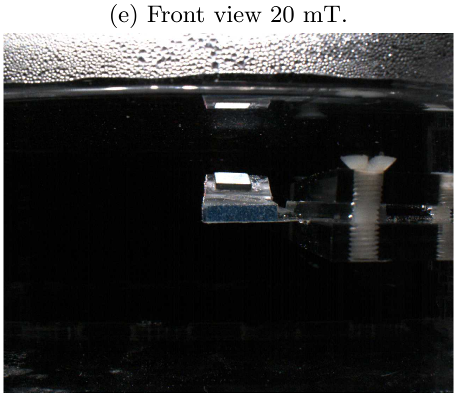

(g) Front view 40 mT.

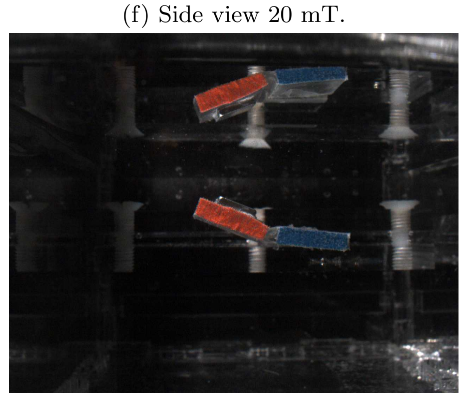

(h) Side view 40 mT.

Figure A.6: Photos taken from the second experiment.

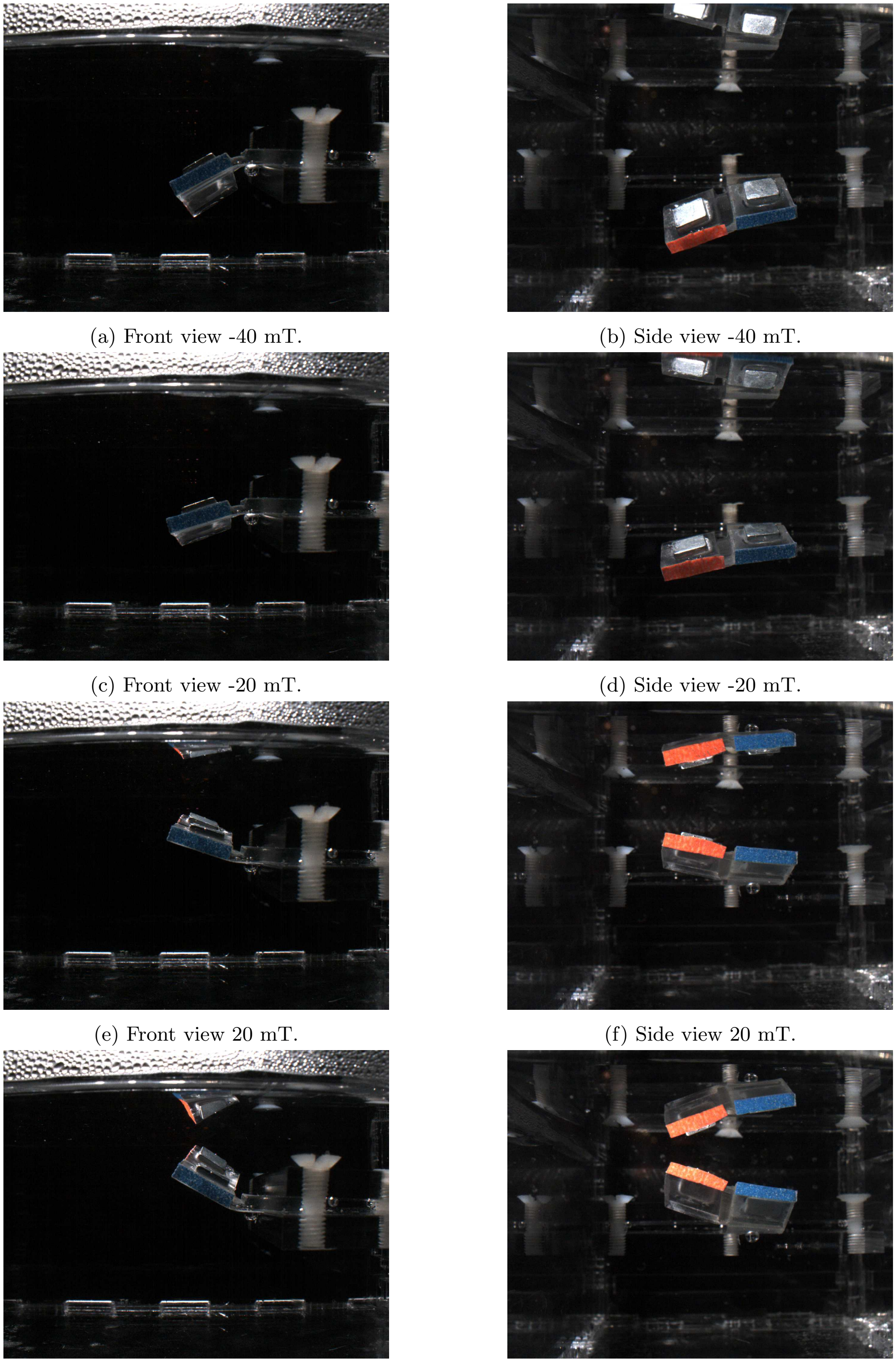

(a) Front view -40 mT.
(b) Side view -40 mT.
(c) Front view -20 mT.
(d) Side view -20 mT.
(e) Front view 20 mT.
(f) Side view 20 mT.
(g) Front view 40 mT.
(h) Side view 40 mT.

Figure A.7: Photos taken from the third experiment.

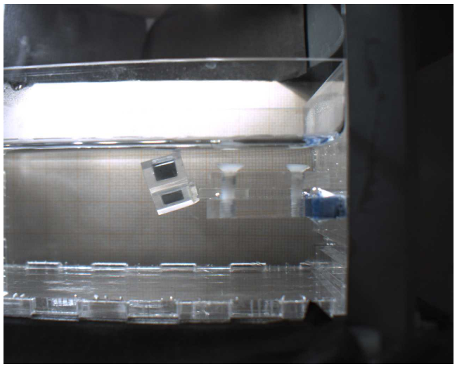

(a) Front view -30 mT.

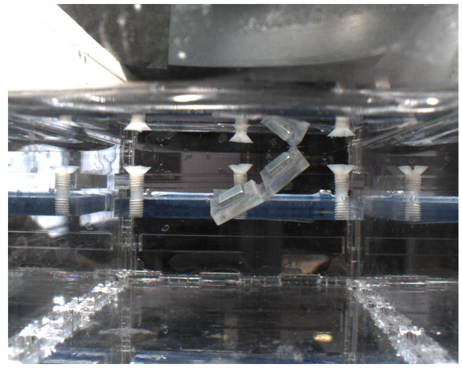

(b) Side view -30 mT.

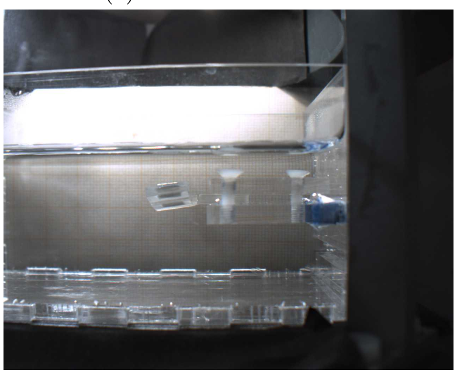

(c) Front view -15 mT.

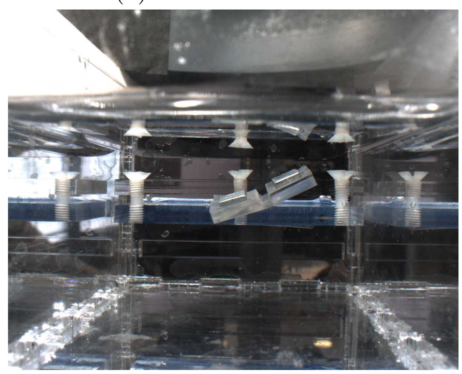

(d) Side view -15 mT.

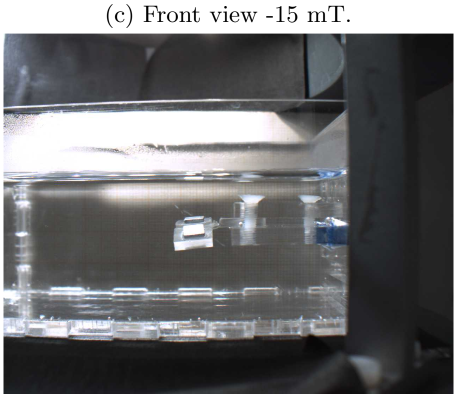

(e) Front view 15 mT.

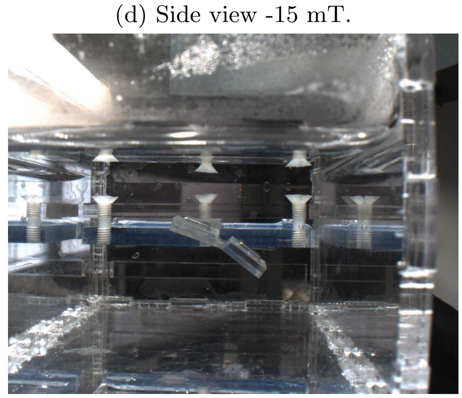

(f) Side view 15 mT.

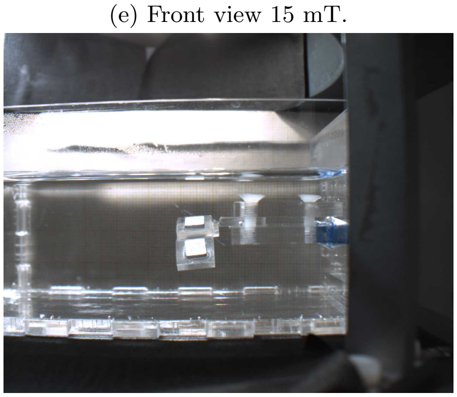

(g) Front view 30 mT.

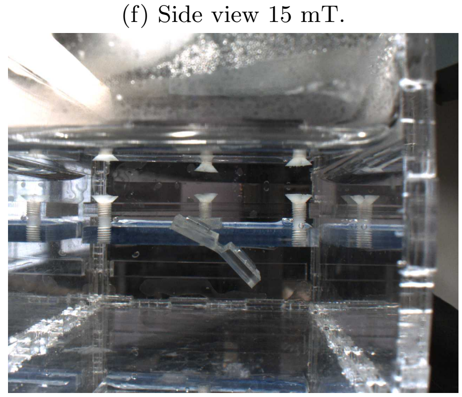

(h) Side view 30 mT.

Figure A.8: Photos taken from a failed experiment.